Probing neutrophils heterogeneity in Glioblastoma: how the metabolism shapes the function of immunosuppressive CD71^{+}Neutrophils

Dipartimento di Medicina Sperimentale

PhD in Network Oncology and Precision Medicine

Dottorando:

Alessio Ugolini, M.D.

Tutor interno:

Prof.ssa Marianna Nuti, Ph.D

Tutor esterno:

Prof. Filippo Veglia, Ph.D

A.A. 2022-23

Table of contents

Abstract

Glioblastoma (GBM) is the most aggressive and lethal form of brain cancer and do not benefit from immunotherapies. These disappointing results may be explained by the strong immunosuppressive tumor microenvironment (TME) that characterize this form of cancer. Neutrophils (Neu) have emerged as key contributors to the TME in different types of cancers, including brain cancers, where their presence is associated with a poor prognosis and a worse response to therapies. Neu represent a heterogeneous population and different subsets of Neu can co-exist in the same cancer patient. However, their characterization remains mainly descriptive in the context of GBM. Moreover, targeting immunosuppressive Neu has proven to be extremely difficult, mostly due to the incomplete understanding of the mechanisms by which Neu can shape the immunosuppressive TME. Histone lactylation (Kla) is a recently described post-translational modification driven by lactate production and able to control the expression of homeostatic and regulative genes during macrophages differentiation. However, the role of Kla in Neu has never been investigated

With this project, we proved that Neu acquire immunosuppressive features within the GBM TME in both human patients and mice models. Single cell RNA sequencing analysis on blood versus tumor derived Neu isolated from GBM-bearing mice, revealed the expansion of a glycolytic subpopulation of Neu within the tumor, characterized by the expression of the transferrin receptor CD71 and by a strong hypoxic signature. Based on the expression of CD71, we identified two different populations of Neu: $CD71^{-}$Neu and $CD71^{+}$Neu. $CD71^{+}$Neu, but not $CD71^{-}$Neu, suppressed T cells responses in mouse and human GBM tumors. Hypoxia induced suppressive activity in $CD71^{+}$Neu via glucose- and lactate-driven histone Kla, which promoted the expression of the potent immunosuppressive enzyme Arginase-1 (ARG-1). $CD71^{+}$Neu were massively mobilized from the bone marrow during tumor progression and quickly infiltrated GBM tumors, where they acquired a proliferative potential and resistance to ferroptosis, thus being able to persist for long periods within the GBM TME. Finally, targeting Kla *in vivo* through

IFNα- or Isosafrole-mediated inhibition of lactate dehydrogenase A (LDHA), resulted in a dramatic improvement of the survival of GBM-bearing mice.

For the first time, these findings bring evidence on Neu heterogeneity in the context of GBM, showing insights on the mechanism that governs the immunosuppressive functions of pro-tumoral Neu. The detrimental role of lactate and Kla in controlling these functions opens a new era for the treatment of GBM patients, offering a novel target to improve the survival and the response to immunotherapies in this cohort of patients.

Background

Glioblastoma

Gliomas are the most common tumors of the central nervous system (CNS) that originate from transformed neural stem or progenitor glial cells. The World Health Organization (WHO) divided gliomas into groups based on histopathological characteristics: low-grade gliomas (LGG, grades I and II) are well differentiated, slow-growing tumors, whereas high-grade gliomas (HGG, grades III and IV) are less differentiated or anaplastic, and strongly infiltrate brain parenchyma[1,2]. Grade IV glioma or Glioblastoma (GBM) is the most aggressive and lethal form of brain cancers, with an incidence of 3.2 cases per 100,000 people per year[3]. Despite surgical resection, targeted radiotherapy and high dose chemotherapy (Temozolomide), patients still have a median overall survival of approximatively 14 months and a 5-year survival rate of less than 3%[4].

In recent years, cancer immunotherapy has revolutionized the way to treat cancer. Immune checkpoint blockade targeting the Programmed cell death protein 1 (PD1)–PD1 ligand 1 (PDL1) axis and/or cytotoxic T lymphocyte- associated antigen 4 (CTLA4) has offered dramatic successes against a variety of solid tumors[5]. However, no survival benefit has been observed in GBM patients[6-8]. These disappointing results may be explained by the strong immunosuppressive tumor microenvironment (TME) that may represent

resistance pathways to immune-mediated interventions[9,10], thus highlighting the urgent need for a more comprehensive understanding of the biology of GBMs.

The brain has long been recognized as an immune privileged tissue because of the restrictions imposed by the brain–blood barrier (BBB)[11]. However, this concept of immune privilege has been partially redefined and now the brain is proposed to be an immunologically distinct rather than an immune privileged organ[6]. It is now clear that there are functional lymphatic vessels in the CNS, and that varied types of leukocytes exist within the CNS[12].

The gliomas present unique transcriptomic profiles, which allows discrimination of classic (CL), mesenchymal (MES), neural (N), and proneural (PN) tumors[2]. Whereas MES gliomas are associated with vascular disorders and with the accumulation of immune cells, PN tumors show a reduced immune infiltration and a better prognosis[13]. The methylation induced by isocitrate dehydrogenases 1/2 (IDH1/2) mutations represses the essential genes necessary for the recruitment and induction of the immune response. Patients with IDH mutation show lower immune infiltrates and better prognosis independently of grade, compared to IDH wild type (WT) gliomas[14].

Acquiring more insights on the mechanisms governing the immunosuppression at the GBM TME is therefore detrimental to develop novel strategies to treat GBM patients and improve their survival.

Neutrophils in GBM

Neutrophils (Neu) are the most abundant circulating leukocytes in humans and they have emerged for their wider functions in the immune response[15]. Recently neutrophils have been described as important players and contributors to the tumoral stroma[16,17] and their presence correlates with a poor prognosis in various cancers[18], including GBM[19-22]. The number of tumor infiltrating neutrophils correlates with glioma grade and represents a negative prognostic parameter for resistant patients[19,23,24]. Neu gene signatures are abundantly present in GBM patients resistant to the anti-PD-1 immunotherapy[25]. Neu

depletion enhanced the survival of mice with brain tumors[26] and the therapeutic efficacy of the anti-PD-1 therapy in a mouse model of glioma[27]. These results indicate that Neu may be an important target to induce anti-tumor responses.

Neutrophils can be commonly found in the tumor core of GBM[6]. IL8, MIF, and CXCL8 lead to neutrophils infiltration at the tumor site[28,29]. Once in the TME, neutrophils release elastase that facilitate neutrophils and glioma cancer cell infiltration at the tumor site[30]. Neutrophils directly promote GBM-initiating cells' proliferation and migration via the production of S100A4, which induced the transition to a mesenchymal phenotype, favoring cancer invasion and resistance to anti-VEGF therapies[31]. Furthermore, neutrophils form neutrophil extracellular traps (NETs) that protect cancer cells in the brain and support the development of both primary tumors and metastasis[32]. Moreover, neutrophils from GBM patients suppress T cells proliferation in an Arginase-1 (ARG-1) dependent manner[33]. Recent evidence showed that tumor damages occurring during early tumor progression may also favor the recruitment of neutrophils to the tumor site and that neutrophils-induced ferroptosis promoted tumor necrosis in glioblastoma progression through a mechanism involving iron-dependent accumulation of lipid peroxides within the tumor[34,35].

Neutrophils are heterogeneous[36] inside the tumor and different subsets of neutrophils can co-exist in the same cancer patient[15,37,38]. At any given moment, myeloid cells in tissues comprise classically activated neutrophils with pro-inflammatory and antitumor activity and pathologically activated polymorphonuclear myeloid derived suppressor cells (PMN-MDSCs) with potent immune suppressive and pro-tumorigenic activity[16,39]. Despite the fact that PMN-MDSCs and neutrophils are different at biochemical, genomic, and functional levels, neutrophils were all classified as either neutrophils or PMN-MDSCs in most of the studies on glioma patients. This limits the clinical relevance of the findings so far reported over the biology of these cells in GBM. In summary, as shown already in other tumors, neutrophils and PMN-MDSCs can coexist in GBM and thus may have different functions in brain tumors. The understanding of the phenotypic and functional

heterogeneity of neutrophils will further clarify their contribution to immune and therapeutic responses to GBM, as well as their clinical relevance.

Scope

Despite the recent appreciation of the functions of different subsets of neutrophils in several types of cancer, the characterization of neutrophils in GBM remains mainly descriptive compared to other myeloid cells. This critically limits the understanding of the cellular and molecular mechanisms used by neutrophils to regulate immune and therapeutic responses in GBM patients. In fact, because of the incomplete understanding of the mechanisms by which Neu can shape the immunosuppressive TME, targeting immunosuppressive Neu has proven to be extremely difficult[40,41].

Thus, our scope was to fill this gap by extensively characterizing Neu heterogeneity in the context of GBM and how GBM can shape Neu function, with the final goal of identifying novel unexplored modalities to treat GBM patients, able to enhance the efficacy of immunotherapies also in this cohort of patients.

Materials and Methods

Human Samples

Samples of peripheral blood and tumor tissues were collected from patients at Moffitt Cancer Center (MCC) (Tampa, Florida) and at Department of Neurology and Neurosurgery at Policlinico Umberto I Hospital (Rome, Italy). The study was approved by Moffitt Cancer Center Institutional Review Board and all patients signed consent forms that were approved by the Institutional Review Board. Samples collected at Department of Neurology and Neurosurgery at Policlinico Umberto I Hospital (Rome, Italy) were collected in accordance with the Declaration of Helsinki and with good clinical practice guidelines and all patients signed informed consent (Policlinico Umberto I Ethics Committee Protocol, RIF.CE: 4181). Blood and Tissue specimens were immediately collected from the operating room and processed as described below.

Clinical Sample Processing

Fresh resected human brain tissue samples were taken within 2 hours to the laboratory to start tissue dissection and processing. Tissue specimens were washed in PBS1x and macro-dissected under sterile conditions. It was further processed with Tumor Dissociation Kit (Miltenyi), according to the manufacturer's instructions, using the gentleMACS Dissociator (Miltenyi). Afterward, the homogenate was filtered through a 70 μm cell strainer and centrifuged at 400 x g for 8 min at 4°C to pellet the cells and myelin. This was followed by myelin removal step by gradient centrifugation with 30% Percoll (Sigma-Aldrich) in 1X PBS (1,592 x g for 30 minutes at 4°C; with slow acceleration and without breaks during deceleration). After myelin (the top white layer) removal, the middle transparent layer and the single-cell suspension was washed in 1X PBS and centrifuged at 400 x g for 8 min at 4°C to pellet the cells. Cells were then used downstream analysis.

Peripheral Blood Mononuclear Cells (PBMCs) were obtained from blood after Percoll gradient stratification for 20 min. at 2000 RPM, RT without break.

Cell lines

GL261 and SB28 cells were obtained from NCI and Hideho Okada at University of California, respectively. They were cultured in RPMI (Gibco) supplemented with 10% fetal bovine serum (Gibco), 1% penicillin/streptomycin (Gibco) and 2-mercaptoethanol 55uM (Gibco). Tumor cell lines were tested negative for mycoplasma contamination.

Mouse models

Animal experiments were approved by the H. Lee Moffitt Cancer Center Animal Care and Use Committee. C57BL/6 mice (female/male, 6–8 weeks old) were purchased from The Jackson Laboratory. Slc2a1 fl/fl Lyz2-cre mice were created after breeding Slc2a1 fl/fl (Slc2a1tm1.1Stma) mice with Lyz2-cre (B6.129P2-Lyz2tm1(cre)Ifo/J). Lyz2-cre (B6.129P2-Lyz2tm1(cre)Ifo/J) mice were obtained from Paulo Rodriguez at Moffitt Cancer Center. Slc2a1 fl/fl (Slc2a1tm1.1Stma) mice were obtained from The Jackson Laboratory. Tfrc fl/fl S100A8-cre mice were created after breeding Tfrc fl/fl (B6.129S(Cg)-Tfrc<tm3.1Nca>/J) mice

with S100A8-cre (B6.Cg-Tg(S100A8-cre,-EGFP)1Ilw/J) mice. Both Tfrc fl/fl (B6.129S(Cg)-Tfrc<tm3.1Nca>/J) mice and S100A8-cre (B6.Cg-Tg(S100A8-cre,-EGFP)1Ilw/J) mice were obtained from The Jackson Laboratory.

Orthotopic glioma cell injection

Mice were intracranially injected with GL261 (40,000 cells) or SB28 (10,000 cells) into the right posterior cortex (1.5 mm posterior from bregma, 1.5 mm lateral from bregma, and 2.5 mm deep) using a stereotactic apparatus. Mice were monitored daily for neurological symptoms, lethargy, and hunched posture that would qualify as signs of tumor burden.

Processing of mouse brain samples

Mice were euthanized with CO2 and perfused with 20 mL of PBS 1X through the left ventricle of the heart using a 25-G needle attached to a 50 mL syringe. Brain tumor tissues were washed in 1X PBS, macro-dissected under sterile conditions and further processed with Tumor Dissociation Kit (Miltenyi), according to the manufacturer's instructions, using the gentleMACS Dissociator (Miltenyi). Afterward, the homogenate was filtered through a 70 μm cell strainer and centrifuged at 400 x g for 8 minutes at 4°C to pellet the cells and myelin. This was followed by myelin removal step by gradient centrifugation with 30% Percoll (Sigma-Aldrich) in 1X PBS (1,592 x g for 30 minutes at 4°C; with slow acceleration and without breaks during deceleration). After myelin (the top white layer) removal, the middle transparent layer and the single-cell suspension were washed in cold PBS and centrifuged at 400 x g for 8 minutes at 4°C to pellet the cells. Cells were counted and then used for downstream analysis.

FACS Sorting

Cells were incubated with a cocktail of surface antibodies, FC-block (BD Biosciences), and Aqua Fixable viability dye (Invitrogen) in FACS (or MACS) buffer (PBS 1x, +1% FBS, +0.5mM EDTA) at room temperature (RT) for 30 min. Afterward, cells were washed with FACS buffer, filtered with 70 μm cell strainer and then target cells were sorted using FACSAria II (BD Biosciences) using FACSDiva (BD Biosciences).

Surface and intracellular staining for flow cytometry

For surface staining, 0.5 × 106 cells were incubated with a cocktail of surface antibodies, FC-block (BD Biosciences), and Aqua Fixable viability dye in FACS Buffer at room temperature (RT) for 30 min. For Intracellular staining, cells were fixed and permeabilized with Fixation/Permeabilization Buffers (BD Biosciences) at 4°C for 15 min, washed twice with Wash Buffer (BD Biosciences), and incubated with a cocktail of intracellular antibody at 4°C for 30 min. Cells were run on either BD FACSymphony (BD Biosciences) or BD LSRII (BD Biosciences), and data were analyzed using FlowJo (Tristar).

Glucose uptake

Cells were incubated with PBS containing 40 μM fluorescent D-glucose analog 2-NBDG (2-[N-(7-nitrobenz-2-oxa-1,3-diazol-4-yl) amino]-2-deoxy D-glucose) (catalog N13195, Life Technologies) for 40 minutes at 37°C. Cells were then washed with cold MACS buffer, stained with surface antibodies for 30 min at 4°C, washed again with cold MACS buffer and fluorescence intensities were immediately analyzed by flow cytometry.

Single cell RNA Sequencing

Mice were injected with 10,000 SB28. After 18 days, neutrophils were sorted from tumor and blood. Blood was collected by submandibular puncture followed by cardiac puncture (right atrium). After blood collection, mice were perfused with 20 mL of PBS 1X through the left ventricle and the tumor was collected and process as previously described. Neu were then FACS sorted in MACS buffer, as previously described. After sorting, Neu were washed in RPMI containing 10% FBS and 1U/μL of Protector RNase inhibitor (Sigma, PN-3335399001). The media was filtered through 0,22 μm before the use. Cells were then counted and resuspended at a concentration of 1,000 cells/μL. 20,000 cells per lane were loaded for encapsulation. Cells were then processed with 10X Chromium 3' scRNA-seq, 40,000 reads/cell using NovaSeq S1-100 and NovaSeq SP-100 sequencing run.

Western blot

Cells were lysed in RIPA buffer (Cell Signaling) in the presence of protease and phosphatase inhibitor cocktail (Thermofisher), 1 mM DTT, Sodium Butyrate (1:100) and 1 mM PMSF, sonicated and stored at −80°C. Whole-cell lysates were prepared and subjected to SDS–PAGE and transferred to PVDF membrane. The membranes were probed overnight at 4°C with primary antibodies. Membranes were washed and incubated for 1h at RT with secondary antibody conjugated with peroxidase. Blots were developed with enhanced chemiluminescence (ECL Millipore) and signals captured with the Odyssey Fc (LI-COR).

CUT&RUN

A diluted aliquot of cells suspension was mixed with Trypan Blue (1:1) and counted on a hemocytometer. Equal numbers of cells were pooled and diluted to a final concentration of 1000 - 300 cells/µL in wash buffer, with 100 µL (~100,000 cells for *in vitro* experiments and ~30,000 cells for *in vivo* experiments) used for each CUT&RUN reaction. CUT&RUN was performed using the CUT&RUN Assay Kit (Cell Signaling) according to the manufacturer's instructions. The DNA was immunoprecipitated with panKla antibody (PTM1401RM, PTM, Bio) or the IgG as non-specific control. The precipitated chromatin DNA was purified using a DNA Clean & Concentrator-5 kit (Zymo Research) and detected by RT-qPCR using specific primers.

Preparation of tumor explant supernatants

Tumor explant supernatants (TES) were prepared from excised mouse and human tumors. A small tumor piece (5–10 mm2) was minced into pieces less than 3 mm in diameter and resuspended in 15-20 mL of RPMI without FBS but supplemented with 1% penicillin/streptomycin. After 16–18 h of incubation at 37°C with 5% CO2, the cell-free supernatant was collected and passed through 0.22-µm filters and stored at −80°C.

Hypoxia

Hypoxic conditions were maintained by generating a 1% O2 and 5% CO2 concentrations through the BioSpherix subchamber system, including a C-Chamber and ProOx C21 Oxygen CO2 Single Chamber Controller.

RT-qPCR.

RNA was extracted using the Quick RNA microprep Kit (Zymo Research) according to the manufacturer's instructions. RNA was DNase-treated and converted to random primed cDNA using Superscript IV kit (Invitrogen). cDNA was used as a template in subsequent PCR with gene-specific primers. RT–qPCR was performed using Power SYBR Green PCR Master Mix (Applied Biosystems) in 96- or 384-well plates. Plates were read with ABI 7900 (Applied Biosystems).

Seahorse analysis

Oxygen consumption rate (OCR) and extracellular acidification rate (ECAR) were measured using a XF96 extracellular flux analyzer (Seahorse Bioscience) through mitochondrial (Mito) and glycolysis (Glyco) stress test. Cells were plated onto CellTak pre-coated wells (1x105cells/well in triplicate) and subjected to mitochondrial stress and glycolysis stress protocols using specific non-buffered XF base mediums. For Mito Stress test, cells were analyzed under basal conditions and in response to 1 μM oligomycin, 2 μM fluorocarbonyl-cyanide-phenylhydrazone (FCCP), and 0.5 μM rotenone/antimycin A. For Glyco Stress Test, cells were plated in XF media lacking glucose and pyruvate and monitored under basal conditions and in response to 10 mM glucose, 1 μM oligomycin, and 50 mM 2-Deoxy-D-glucose (2-DG).

Lactate colorimetric assay

Intracellular lactate concentrations were assessed using a Lactate colorimetric Assay Kit II (Sigma).

Pimonidazole

HypoxiprobeTM-1 [Pimonidazole Hydrochloride] solution was injected intraperitoneally at a dosage of 60 mg/kg. 1 hour after injection, mice were euthanized and tissues were collected. After tissue processing, single cell suspensions were stained for surface antigens and, subsequently, were processed for the intracellular staining. A purified rabbit anti-pimonidazole (Pab2627AP) was used at a 1:50 dilution (60 min. at RT) for the intracellular staining, followed by a Secondary APC-conjugated anti-rabbit staining (30 min. at RT).

BrdU

Mice were stereotactically injected with SB28 cell line (10,000 cells/mouse). 15 days after the tumor cells injection, a one-time administration of BrdU was performed. APC BrdU Flow Kit (BD PharmigenTM, Catalog No. 552598) was used, following manufacturer's instructions. Briefly, 165 μL of BrdU solution (1.65 mg) were intraperitoneally injected in each mouse at day 0. Mice were euthanized either 3 hours post injection (D0) or 9 days post injection (D9) and tissues were collected and processed to obtain single cell suspensions. Surface staining was first performed (30 min. at RT). Cells were then washed, resuspended in 100 μL of BD Cytofix/CytoPerm Buffer and incubated for 30 min on ice. Cells were washed with 1 mL of 1X BD Perm/Wash Buffer. Cells were then resuspended in 100 μL of BD CytoPerm Permeabilization Buffer and incubated for 10 min. on ice, washed with 1X BD Perm/Wash Buffer, re-fixed for 5 minutes on ice with 100 μL of BD Cytofix/CytoPerm Buffer and then washed with 1X BD Perm/Wash Buffer. Cells were then resuspended in 100 μL of diluted DNase (300 μg/mL in PBS 1X) and incubated for 1 hour at 37°C, then washed with 1X BD Perm/Wash Buffer. Cells were then stained with the anti-BrdU (1:40) for 20 min. at RT. Cells were finally acquired using a low/medium flow rate, no greater than 400 events/second.

LiperFluo staining

Single cells suspensions were first stained for surface antigens and then washed in 1X PBS. Supernatant was carefully discarded in order to remove all the FBS. Cells were then

resuspended in 100 μL of 1X PBS and 10 μM of Liperfluo (Dojindo) was added to each sample; cells were incubated for 30 min. at 37°C and then washed with 1X PBS.

Generation of murine neutrophils for *in vitro* studies

To get mature neutrophils, femur and tibiae of naïve C57BL/6 mice (female/male, 6–8 weeks old) were flushed with FACS Buffer; BM cells were then filtered through a 70mM cell strainer and red blood cells were lysed with the ACK Lysing Buffer. 3 mL of Histopaque 1119 were added to a 15 mL tube followed by 3 mL of Histopaque 1077; then, BM cells were resuspended in 1 mL of cold 1X PBS and carefully added on top. Tube was centrifuged for 30 min., 872 xg at 4°C with no break. Bottom white layer was collected and stained with an anti-Ly6G to check purity (only samples containing > 95% of neutrophils were used for further experiments).

To generate in vitro $CD71^{-}$Neutrophils and $CD71^{+}$Neutrophils, BM cells were cultured for 5 days with GM-CSF. Briefly, femur and tibiae of naïve C57BL/6 mice (female/male, 6–8 weeks old) were flushed with cold FACS Buffer; BM cells were then filtered through a 70mM cell strainer and red blood cells were lysed with the ACK Lysing Buffer. Cells were seeded at a concentration of $3x10^5$ cells/mL in 6-well plates, 3 mL/well with 20 ng/mL of GM-CSF (Peprotech) at day 0 either in normoxic or hypoxic conditions. At day 3, GM-CSF was added to the culture in 1 mL of fresh complete RPMI. In TES experiments, 30% of TES was added to the cultures at day 0 and day 3. In some experiments, cells were treated with 2-Deoxy-D-glucose (2-DG) 5 mM at day 4, LDHA inhibitor (GNE-140) 5 μM at day 3 and 10 μM at day 4, ACLY inhibitor (BMS-303141) 20 μM at day 3 and 4, IFNα (Miltenyi) 12,000 U.I./mL at day 3, Isosafrole (Chem Service) 250 μM at day 3.

Generation of human neutrophils for *in vitro* studies

To get human blood neutrophils, 15 mL of Histopaque 1119 were added to a 50 mL tube followed by 15 mL of Histopaque 1077; then, 15 mL of blood were carefully added on top. Tube was centrifuged for 30 min., 872 xg at 4°C with no break. Bottom white layer was collected and stained with an anti-CD66b to check purity (only samples containing > 95% of neutrophils were used for further experiments).

Suppression assay, mini-suppression assay and IFN-γ production

MOUSE SUPPRESSION ASSAY AND IFN-γ PRODUCTION

U-bottom 96-well plates were used. Anti-CD3 (Invitrogen, clone 145-2C11) and anti-CD28 (Invitrogen, clone 37.51) were diluted at a final concentration of 1 μg/ml in sterile PBS 1X. 50 μl of PBS containing the antibodies were loaded in each well (one or two for each condition). 2 wells were kept as negative control (no antibodies) and 2 wells as positive control. The plate was incubated at 37°C for 4-6 hours.

For T cells insolation, one spleen was mechanically dissociated and $CD3^+$ cells were isolated with a negative selection kit (Mojo Sort, Biolegend). A maximum of $10x10^6$ isolated T cells were resuspended in 1 mL of sterile PBS 1X + 0,1% FBS containing 0.3 μM CFSE (BioLegend) and incubate for 10 min in the dark at RT. T cells were then washed twice with cold RPMI complete, 5 min 1500 rpm at 4°C. Isolated T cells were resuspended in fresh RPMI complete, containing 10% FBS, Pen/Strep 1:100 and β-Mercaptoethanol 1:1000. For in vitro suppression assays, T cells were resuspended at a concentration of 0.5-1 $x10^6$ cells/mL.

For in vitro suppression assays, neutrophils were FACS sorted, washed with fresh RPMI complete, counted and resuspended at the same concentration of T cells (0.5-1 $x10^6$ cells/mL) in fresh complete RPMI.

PBS was removed from the wells by turning the plate upside down and shaking it and the wells were washed twice with 200 μl of PBS by repeating this step. Depending on the experiment, 50,000 (50 μl) or 100,000 (100 μl) T cells were plated in each well. Neutrophils were added in the same amount and volume of T cells in order to get a ratio of 1:1 (except from the negative and positive control wells, where complete media was instead added). Surrounding empty wells were filled with 200μl of PBS to avoid evaporation. T cells proliferation was analyzed after 72h.

For IFN-γ production experiments, 66 hours after plating the cells, cells were re-stimulated with the Cell activation cocktail, containing PMA and ionomycin (BioLegend), at a

concentration of 2 μl/mL and with Golgi Stop (BD Biosciences) at a concentration of 2μl/3mL. 6 hours after, cells were first stained for surface antigens and then processed for intracellular staining and stained with a PE anti-IFN-γ 1:100 for 30 min. at 4°C. IFN-γ production was then analyzed by flow cytometry.

For the suppression assays with the Arginase-1 inhibitor Nω-Hydroxy-nor-L-arginine (norNOHA, Sigma), T cells and neutrophils were resuspended at a concentration of 0.5 x10^6 cells/mL and 25,000 cells (50 μl) of each were used for the assay. NorNOHA was added at a concentration of 750 μM. Since norNOHA can partially reduce T cells proliferation, it has been added also to positive controls.

HUMAN SUPPRESSION ASSAY

U-bottom 96-well plates were used. Anti-CD3 (clone UCHT1; BD Biosciences) was diluted at a final concentration of 20 μg/ml in sterile PBS 1X. 50 μl of PBS containing the antibodies were loaded in each well (one or two for each condition). 2 wells were kept as negative control (no antibodies) and 2 wells as positive control. The plate was incubated at 37°C for 4-6 hours.

For T cells isolation, PBMC from the same donor of neutrophils were collected from whole blood and T cells were isolated using the Human $CD3^+$ T Cell Enrichment Column Kit (R&D Systems), stained with CFSE and resuspended in fresh complete RPMI, containing 10% FBS and Pen/Strep 1:100.

Neutrophils were FACS sorted and resuspended in fresh complete RPMI.

PBS was removed from the wells by turning the plate upside down and shaking it and the wells were washed twice with 200 μl of PBS by repeating this step. T cells and neutrophils were added at a 1:1 ratio. 2 μg/ml of soluble anti-CD28 (clone CD28.2; BD Biosciences) were added in each well (except for negative control). T cells proliferation was analyzed after 72h by flow cytometry.

EX-VIVO MINI-SUPPRESSION ASSAY

For both mouse and human *ex vivo* mini-suppression assays, neutrophils were sorted in FACS buffer, washed in fresh complete RPMI, resuspended in 500 µl of complete RPMI and counted. Neutrophils were then washed, supernatant was completely discarded and cells were resuspended at a concentration as low as 5,000 cells/50µl (between 5,000 and 20,000 /50µl). T cells were resuspended at the same concentration of neutrophils, and used for the mini-suppression assay at a 1:1 ratio, in a final volume per well of 100 µl (50 µl of neutrophils and 50 µl of T cells).

Giemsa staining

Sorted neutrophils were cytospinned on the slides. Slides were fixed in methanol 5-7 minutes. Giemsa Stain was diluted 1:20 with deionized water. Slides were stained for 45 minutes, rinsed 3 times with deionized water and a cover was mounted with Cytoseal-60 Mounting media.

In vivo treatments

For all the *in vivo* treatments, 10,000 SB28 were injected. For Neu depletion, we performed intraperitoneal (i.p.) injections of a rat anti-LY6G antibody (BE0075-1, 200 µg/mouse) combined to an anti-rat antibody (BE0122, 50 µg/mouse)[42] every other day starting at day 8. IFNα (Miltenyi, 130-093-131) was administered i.p. in 100 µL of PBS 1X per mouse at a dose of $1x10^4$ I.U./mouse, every day starting from D7. Isosafrole (ChemServive, N-12281) was administered i.p. in 200 µL of 1% Carboxymethylcellulose (prepared in saline solution) per mouse at a dose of 200 mg/kg, every other day starting from day 7. The respective isotypes and vehicles were used as controls for each experiment.

Statistical analysis

After testing for normal distribution of data, statistical analyses were performed using two-tailed Student's *t* test; paired *t* test was used for matched samples; when more than two groups were compared, one- or two-way ANOVA test with correction for multiple comparisons (Tukey or Holm-Šidák post hoc test) were used. Data were presented as mean ± SEM. Pearson Correlation Coefficient with the associated two-tailed *p* value was calculated to study correlations. Kaplan-Meier plots were used for survival analysis, and

the log rank test was used to compare survival distributions between groups. A p <0.05 was considered statistically significant.

Results

Neutrophils infiltrate brain tumors acquiring immunosuppressive features

To understand the role of neutrophils in brain cancer, we first analyze the abundance of neutrophils in different orthotopic models of brain tumor (GL261 and SB28) by flow cytometry. We observed a higher frequency of neutrophils in spleen of GL261 and SB28 models than in spleen of tumor free mice injected with vehicle (naïve) (**Fig. S1a**), while the frequency of neutrophils was unchanged in the bone marrow (BM) of GL261 and SB28 models, compared to naïve mice (**Fig. S1a**). Even though the frequency of neutrophils in spleen in both models was higher than in naïve mice, SB28 tumors showed a much higher infiltration of neutrophils compared to GL261 tumors (**Fig. 1a**). The frequency of neutrophils in GL261 tumors was only slightly, but not significantly, higher to that observed in naïve brain. Of note, contrary to GL261, SB28 brain tumors recapitulate key characteristics of human GBMs, such as aggressive growth and low mutation burden, and exhibited high resistance to immune checkpoint blockade therapy[43]. We next analyzed the kinetics of neutrophil infiltration in GBM tumors. In both tumor models, we found that neutrophils were not expanded at early stages (day 12) but critically infiltrated GBM tumors at late stages (day 21 and day 24) (**Fig. 1b**). To assess the contribution of neutrophils to tumor growth, we analyzed the survival of mice with brain tumors (SB28) upon depletion of total neutrophils using an optimized approach for a durable neutrophils' depletion, based on the administration of a rat anti-LY6G antibody combined to an anti-rat antibody[42]. Neutrophils' depletion was effective both in the blood (at early and late stages) and inside the tumor (**Fig. S1b, c**). To make sure that neutrophils depletion was truly effective and not just the result of the depleting antibody covering the receptor, an indirect neutrophils' staining ($CD11B^{high}$ $F480^{-}$ $LY6C^{int}$), not including Ly6G, was used to validate our observations (**Fig. S1b, c**). Similarly to what has been previously published[26], we found that SB28-bearing mice survived longer upon neutrophils'

depletion, when compared to control mice treated with the isotype controls (**Fig. 1c**). Interestingly, the depletion of neutrophils was associated with a higher infiltration of both $CD8^+$ and $CD4^+$ T cells inside GBM tumors (**Fig. 1d**). Of note, the frequency of other potentially immunosuppressive myeloid cells (including monocytes, monocyte derived macrophages, MDM, and microglia, MG) was not altered by this depletion strategy (**Fig. S1d**).

Since it is established that neutrophils can acquire immunosuppressive functions in cancer[15], we analyzed the immunosuppressive ability of neutrophils isolated from mouse SB28 tumors. To test the functionality of neutrophils, we FACS sorted neutrophils ($LY6G^{high}$ $LY6C^{lo/-}$ CD11b+ $F4/80^{lo/-}$) from bone marrow (BM), spleen and brain tumors, and we co-cultured them with autologous $CD3^+$ T cells pre-stained with CFSE and activated with anti-CD3/CD28 antibodies. Contrary to BM and spleen derived neutrophils, which lacked suppressive ability, neutrophils from tumors were able to suppress the proliferation of both $CD4^+$ and $CD8^+$ T cells (**Fig. 1e**). The acquisition of suppressive activity correlated with an immunosuppressive signature, characterized by high mRNA levels of different immunosuppressive genes such as arginase-1 (*arg1*), nitric oxide synthetase 2 (*nos2*), nicotinamide adenine dinucleotide phosphate oxidase 2 (*nox2*) and Programmed Death Ligand 1 (*pdl1*) compared to BM and spleen derived neutrophils (**Fig. S1e**).

To assess the relevance of neutrophils in human patients we analyzed the frequency of neutrophils in human brain tumors by flow cytometry. We observed that neutrophils infiltrated human brain tumors to a similar extent of what was previously observed in the SB28 mouse model, accounting for 10-20% (with some patients showing frequencies up to 70%) of the $CD45^+$ immune cells population and representing one of the most expanded immune populations in human brain tumors (**Fig. 1f, g**). We did not find differences in the frequency of neutrophils between diagnosed (ND) to recurrent (REC) brain tumors (**Fig. 1h**). However, we found an increased, even if not statistically significant, frequency of neutrophils in GBM tumors compared to oligodendrogliomas and astrocytomas (**Fig. 1i**).

Of note, GBM has a worse prognosis than oligodendroglioma and astrocytoma tumors[44]. Next, we FACS sorted neutrophils from blood and tumors of brain tumor patients, and we co-cultured them with autologous T cells, pre-stained with CFSE and stimulated with anti-CD3/CD28 antibodies. As previously observed in the SB28 mouse model, neutrophils from tumors suppressed the proliferation of $CD4^+$ and $CD8^+$ T cells compared to blood derived neutrophils, which lacked suppressive properties (**Fig. 1j**). The suppressive activity of tumor associated neutrophils correlated with a higher expression of the Lectin-Like Oxidized Low-Density Lipoprotein Receptor 1 (LOX-1) (**Fig. S1e**), which has already been described as highly expressed by immunosuppressive neutrophils in other tumor models[34]. Moreover, a higher frequency of neutrophils in brain tumor tissues inversely correlated with the infiltration of total $CD3^+$ T cells, $CD4^+$ T cells and $CD8^+$ T cells (**Fig. 1k**).

Collectively, our data may suggest that local clues provided by mouse and human brain tumors favor the reprogramming of neutrophils towards cells with potent immunosuppressive activity.

A population of glycolytic neutrophils expressing the CD71 receptor is expanded in brain tumors where it acquires a hypoxic signature.

Neutrophils are known to be heterogeneous inside the tumor[15]. Thus, to probe neutrophils' heterogeneity in brain tumor, we employed single cell RNA sequencing (scRNA-seq). Single-cell analysis of neutrophils generally remains a significant challenge. This is because neutrophils have relatively low RNA content and relatively high levels of RNases and other inhibitory compounds, resulting in fewer transcripts detected in GEMs, and less usable sequencing reads. Furthermore, neutrophils are particularly sensitive to degradation after collection and processing. Thus, we optimized the samples' collection and processing, as described in the materials and methods section, in order to obtain a high quality 10x Genomics Single-Cell Assays for neutrophils. Therefore, we FACS sorted neutrophils ($CD45^+Ly6G^+Ly6C^{low/-}$) from blood and tumor of 4 SB28-bearing mice and we pulled them together in couples, obtaining 4 different samples (blood Neu_1, blood Neu_2, tumor Neu_1, tumor Neu_2) that were processed for 10X Chromium 3' scRNA-

seq, with 40,000 reads per cell. Cells with less than 200 detected genes, or more than 15% mitochondrial genes, or log10GenesPerUMI <0.8 were removed. Also, three methods were used to predict doublet (or multiplets) cells (scrublet, scDblFinder, and DoubletFinder). Cells predicted as doublets in >=2 methods were removed. In total, 18,493 single cells were considered and processed for further analysis. The scran[45] and scater[46] packages were used to normalize the raw counts to control cell-specific biases. These normalized counts were then supplied to Seurat package (v3.1.1)[47] to perform batch correction, clustering, and marker identification for the predicted cell clusters. To determine cell identity, we matched our dataset with two separate public mouse datasets[48,49] using singleR package (v1.0.0)[50]. Based on transcriptomic results, we projected them into two dimensions with Uniform Manifold Approximation and Projection (UMAP)[51]. Only cells expressing the neutrophils' signature were selected for further analysis. Unbiased, graph-based clustering initially identified 24 different clusters (**Fig. S2a**). Based on similar gene signatures (**Fig. S2b**), the 24 clusters were subsequently re-classified in 9 sub-population of neutrophils (celltype_1 to 9, **Fig. 2a** and **S2c**). Blood derived neutrophils clustered together and were well separated from tumor derived neutrophils (**Fig 2b**). Using computational trajectory analysis, we assessed the relationship between blood and tumor derived neutrophils. Blood neutrophils were used as the initial stage for the trajectory, assuming that the pseudotime reflects a direction of possible transition from blood neutrophils to tumor neutrophils. Interestingly, trajectory analysis revealed that blood derived neutrophils can give raise to tumor derived neutrophils, most likely indicating that blood neutrophils migrate to the tumor and that the tumor microenvironment shapes neutrophils phenotype producing different sub-populations of tumor associated neutrophils. Then, the 9 sub-populations of neutrophils were studied and classified based on their peculiar features and markers expression (**Fig. 2c**). Celltype_1 was referred as the conventional neutrophils population and represented more than 90% of blood neutrophils (**Fig. 2d**). It was characterized by the expression of *Lyz2* and *Rac2* and appeared to be dependent on oxidative phosphorylation (**Fig. 2e**). Celltype_2 represented a very small sub-population of neutrophils, characterized by the expression of *Adpgk* and *Camp* and a high metabolic

signature (**Fig. 2c, d, e**). Celltype_3 was referred as the glycolytic sub-population of neutrophils (**Fig. 2c**). In fact, compared to the other sub-populations, it showed a higher expression of the glycolytic pathway (**Fig. 2e**) and of all the genes involved in the glycolysis, including the solute carrier family 2 member 1, *Slc2a1* (GLUT-1, **Fig. S2b**) and the lactate dehydrogenase A, *Ldha*, which was preferentially expressed by this sub-population and thus considered as a specific marker (**Fig. 2c** and **S2b**). Interestingly, the 4 clusters forming the Celltype_3 (clusters 2, 4, 13 and 16) exclusively expressed the transferrin receptor *Tfrc* (CD71, **Fig. S2b**) that was thus considered as another specific marker of this population (**Fig. 2c**). Celltype_3 was the sub-population most expanded in the tumor when compared to the blood (**Fig. 2d**) and was the most enriched for the hypoxia pathway (**Fig. 2e**), suggesting its localization in the hypoxic regions of the tumor. In addition, this population showed an increased unfolded protein response, fatty acid metabolism and TGFβ signaling (**Fig. 2e**), all features that were previously associated with an immunosuppressive phenotype of neutrophils[16,39,52]. Celltype_4, regarded as the pro-inflammatory sub-population and characterized by the expression of *Cxcl3* and *Fpr1* (**Fig. 2c**), was represented in both the blood and the tumor, being expanded mostly in the latter (**Fig. 2d**). Similarly to the Celltype_3, the Celltype_4 showed an enrichment for the hypoxic pathway (**Fig. 2e**). Being this sub-population the second most represented in the tumor after Celltype_3 and being the GBM one of the most hypoxic tumor types[53,54], it suggests that the greatest part of brain tumor associated neutrophils is found in hypoxic regions. Celltype_5 was characterized by the exclusive expression of *Bcl2l15*, was represented in both the blood and tumor, but more expanded in the latter; differently from the previous 2 sub-populations, Celltype_5 was not enriched for the hypoxic pathway. Celltype_6 was equally represented in both the blood and tumor, was identified by the expression of *Ifit* and referred as the Interferon response subpopulation (**Fig. 2c, d, e**). Celltype_7 was a low count subtype (**Fig. 2c**). Celltype_8, regarded as the stress response and identified by the expression of *Eif5a* and *Atf3*, was mostly expanded in the tumor and, similarly to Celltype_3 and Celltype_4, was enriched for the hypoxic pathway (**Fig. 2c, d, e**). Celltype_9 represented a sub-population of activated neutrophils, characterized by the

expression of *CD63* and *Ccrl2* and, even if only little represented, was only found inside the tumor (**Fig. 2c, d, e**).

Altogether, our scRNA-seq data indicates that blood neutrophils migrate inside brain tumors, where different stimuli can shape their phenotype, giving raise to different sub-populations. Most of the tumor associated neutrophils are exposed to hypoxic conditions in the context of brain tumor. A sub-population of highly glycolytic neutrophils, mostly expanded inside the tumor, can be identified by the expression of CD71 and shows a highly enriched hypoxic signature together with other signatures previously associated with immunosuppressive neutrophils.

CD71^{+}Neu are critical contributors to the immunosuppressive activity associated with neutrophils in brain tumors.

To validate the observations made with the scRNA-seq, we studied the expression of CD71 by both flow cytometry and RT-qPCR. The immunosuppressive activity of tumor infiltrating neutrophils correlated with a higher expression of CD71 (encoded by the *tfrc* gene) compared to BM and spleen neutrophils isolated either from mice with brain tumors or naïve mice, by both RT-qPCR (**Fig. S3a**) and flow cytometry (**Fig. 3a**). CD71 is a transferrin receptor that was associated with the earliest neutrophils developmental stages in the bone marrow[55]. CD71 marked proliferating neutrophils, which were expanded in the blood of melanoma patients and detectable in blood and tumors from lung cancer patients[55]. Based on the expression of CD71, we were able to identify two main populations of neutrophils by flow cytometry in murine brain tumor models: CD71^{-} Neutrophils (CD71^{-}Neu) and CD71^{+}Neutrophils (CD71^{+}Neu) (**Fig. 3b**). CD71^{+}Neu were previously reported as immature neutrophils characterized by the double expression of CD71 and CD117[55]. In our case, both CD71^{-}Neu and CD71^{+}Neu showed the characteristic morphology of nuclei associated with polymorphonuclear mature neutrophils. In line with previous reports, CD71^{+}Neu showed a higher expression of CD117, which suggested an immature phenotype[55] (**Fig. S3b**). However, they also showed a higher expression of CD101, LY6G and CD11B (**Fig. S3b**), suggesting common features of both mature and

immature tumor associated neutrophils and an activated phenotype[15]. CD71$^+$Neu were mostly found inside GBM tumors, where they accounted for about 20-30% of total neutrophils (**Fig. 3d**). In spleen and BM, they represented about 1% and 6% of total neutrophils, respectively (**Fig. 3d**). Blood neutrophils were similar to splenic Neu regarding CD71 expression (data not shown). The proportion of CD71$^+$Neu in total BM, spleen, and tumor neutrophils was similar to what observed in BM, spleen and brain of naïve mice, respectively (**Fig. 3d**). Next, to assess if there is an expansion of CD71$^+$Neu in GBM tumors, we analyzed the frequency of CD71$^+$Neu out of CD45$^+$ immune cells in spleen, BM and tumor tissues in both GL261 and SB28 murine GBM models and compared the two models to naïve mice. The percentage of CD71$^+$Neu out of CD45$^+$ immune cells in SB28 brain tumors was significantly higher than in naïve brain tissue and GL261 brain tumors (**Fig. 3e**). However, the frequencies of CD71$^+$Neu in BM and spleen of SB28 model were similar to the ones observed in BM and spleen of both naïve mice and GL261 model (**Fig. S3c**). Of note, the frequency of CD71$^+$Neu out of CD45$^+$ cells in the BM was similar to the one observed in the tumor and higher than the one observed in the spleen; this seems in line with the previous reports that described the CD71 as a receptor expressed by neutrophils at an early stage of their development and, thus, the CD71$^+$Neu population as more represented in the BM. Next, we found that CD71$^+$Neu were mostly found in GBM tumors at later stages of tumor progression in SB28 model (**Fig. 3f**), similarly to what was previously observed for the total neutrophils population (**Fig. 1b**). Since from the scRNA-seq data CD71$^+$Neu showed features associated with immunosuppressive Neu, we investigated their contribution to the immunosuppressive ability of GBM associated Neu that was previously described. To assess the function of CD71$^+$Neu, we FACS sorted these cells from SB28 tumors and tested their ability to suppress the proliferation of CD4$^+$ and CD8$^+$ T cells stimulated with an anti-CD3 and anti-CD28. To perform *ex vivo* suppression assays with low numbers of neutrophils, we optimized a neutrophils-based mini-suppression assay, as described in the Materials and Methods section. We found that CD71$^+$Neu were potent immunosuppressive cells compared to CD71$^-$Neu, which showed a very mild to inexistent suppressive activity (**Fig. 3g**). Of note, BM derived CD71$^+$Neu and

CD71$^-$Neu lacked any suppressive activity (**Fig. S3d**), indicating that the GBM TME can shape CD71$^+$Neu function. The immunosuppressive activity of tumor derived CD71$^+$Neu was associated with a pro-tumoral signature, characterized by a higher expression of *arg1*, *vegfa*, *tgfb*, PDL-1 and CD14[37] (**Fig. S3e**). To clarify the role of CD71 in the regulation of the immunosuppressive activity of neutrophils in GBM tumors, we created neutrophils-specific conditional knock-out mice (CKO) deficient in *tfrc* (CD71) by crossing Tfrc$^{fl/fl}$ mice with S100A8 Cre$^+$ mice (Tfrc Cre$^+$). Brain tumors (SB28) were established in Tfrc Cre$^+$ and Cre$^-$ mice and total neutrophils, which were FACS sorted from tumors, were assayed for their ability to suppress the proliferation of CD4$^+$ and CD8$^+$ T cells. First, we confirmed the efficient KO by WB on *ex-vivo* FACS sorted neutrophils (**Fig. S3f**). Second, no survival advantage was observed for Tfrc Cre$^+$ SB28-bearing mice (**Fig. S3g**). Third, we found that CD71 CKO neutrophils suppressed the proliferation of CD4$^+$ and CD8$^+$ T cells at same extent of control neutrophils (Tfrc Cre$^-$) (**Fig. S3h**), suggesting that CD71 is not involved in the regulation of immunosuppressive activity of neutrophils in GBM tumors.

To assess the relevance of our data, we analyzed the expression of CD71 in blood and tumor neutrophils from patients with brain cancer. Similarly to what we observed in mice models, we were able to identify 2 distinct populations of Neu based on CD71 expression also in humans (**Fig. 3h**). We also found that the expression of CD71 was higher in neutrophils isolated from brain tumors compared to blood (**Fig. 3h**). CD71$^+$Neu represented 10-20% of total neutrophils that infiltrated human GBM tumors. In blood, CD71$^+$Neu represented 2-5% of total neutrophils. This proportion was similar to that observed in healthy donors' blood. When we separated our brain cancer patients based on the diagnosis, we observed that CD71$^+$Neu infiltrated GBMs to a higher extent than Oligodendrogliomas and, even if not statistically significant, Astrocytomas (**Fig. 3i**). Of note, Oligodendrogliomas have the best prognosis between the three groups and GBMs the worst[44]. Next, we asked whether human CD71$^+$Neu are suppressive cells as in mouse models. Towards this goal, we FACS sorted CD71$^+$Neu from blood and tumor tissue of patients with brain tumors and we co-cultured them with autologous CD4$^+$ and CD8$^+$ T cells, pre-stained with CFSE and stimulated with anti-CD3/CD28 antibodies. We found

that CD71$^+$Neu from tumors highly suppressed the proliferation of T cells, compared to CD71$^-$Neu (**Fig. 3j**). However, CD71$^+$Neu isolated from blood of the same brain tumor patients lacked suppressive functions (**Fig. S3i**). Importantly, the suppressive activity of tumor CD71$^+$Neu was associated with high expression of the pro-tumoral markers arg*1*, *tgfb*, PDL-1 and LOX1 compared to tumor CD71$^-$Neu (**Fig. S3j**). Moreover, the frequency of CD71$^+$Neu, but not of CD71$^-$Neu, negatively correlated with the presence of the activated anti-tumoral population CD8$^+$PD1$^+$CD137$^+$ T cells (**Fig. 3k**). Importantly, recent papers showed that the density of CD8$^+$PD1$^+$CD137$^+$ T cells correlated with improved responses to immune checkpoint blockade therapies in different cancer types[56-58].

Altogether, our data suggest that CD71$^+$Neu represent critical contributors to the immunosuppressive ability of neutrophils in mouse and human brain tumors.

Hypoxia drives immunosuppressive function and ARG-1 expression in CD71$^+$Neu.

Our data showed that CD71 was highly expressed by tumor infiltrating neutrophils, thus we asked whether the GBM TME may drive the expression of CD71 in Neu and consequently their suppressive functions. To reproduce GBM TME *in vitro*, we used brain tumor explant supernatant (TES) and hypoxia. Hypoxia is a crucial factor in GBM TME and our scRNA-seq data showed that most of GBM associated Neu, and CD71$^+$Neu in particular, are exposed to hypoxia. To confirm these findings, we injected pimonidazole (PIMO), a hypoxia tracer, in SB28-bearing mice before the sacrifice, and then performed an anti-PIMO intracellular staining to assess whether tumor associated neutrophils experience hypoxia. We found that both CD71$^-$Neu and CD71$^+$Neu are exposed to hypoxia in GBM tumors (**Fig. 4a**). Hypoxia can induce CD71 expression in tumor cells as early as 6 hours[59,60]. Thus, we treated naïve mature neutrophils, isolated from bone marrow or spleen (data not shown) through histopaque gradient, with TES or hypoxia (1% O2), for up to 24 hours. Of note, more than 95% of Neu isolated through histopaque gradient were CD71$^-$ Neu (**Fig. S4a**). We observed that neither TES nor hypoxia were able to induce the expression of CD71 by flow cytometry (**Fig. S4a**), RT-qPCR (**Fig. S4b**) and WB (**Fig. S4c**) at

different time points. We found similar results when we analyzed the expression of CD71 by flow cytometry in mature neutrophils isolated through histopaque gradient from blood of human GBM patients and exposed to hypoxia (**Fig. S4d**). Moreover, mouse and human $CD71^{-}$Neu isolated through histopaque gradient did not acquire suppressive activity upon stimulation with TES or hypoxia (data not shown). Then, in order to get both $CD71^{-}$Neu and $CD71^{+}$Neu and study the effects of the TME on these cells *in vitro*, we decided to generate neutrophils by culturing mouse total BM cells with GM-CSF for 5 days, in the presence of TES or hypoxia (1% O2). First, through this system, we were able to generate a significant amount of $CD71^{+}$Neu (**Fig. 4b** and **S4e**), regardless of the presence of TES or hypoxia, indicating that TES and hypoxia neither drive the expansion of this population from hematopoietic progenitors nor increase the CD71 expression throughout neutrophils differentiation. Normoxic $CD71^{+}$Neu expressed significantly lower levels of LY6G compared to normoxic $CD71^{-}$Neu, confirming that in normoxic conditions the CD71 receptor is expressed mostly in immature neutrophils (**Fig. 4c**). However, hypoxia was able to induce a significant increase of both LY6G and CD11B on $CD71^{+}$Neu (**Fig. 4c**), partially mimicking the phenotype observed *in vivo* within the TME and suggesting that hypoxia may induce the maturation and activation of the $CD71^{+}$Neu population, although maintaining the expression of CD71. Next, we used our *in vitro* model to FACS sort $CD71^{-}$Neu and $CD71^{+}$Neu and we co-cultured them with $CD4^{+}$ and $CD8^{+}$ T cells pre-stained with CFSE and stimulated with an anti-CD3 and anti-CD28 to assess their ability to suppress the proliferation and the IFN-γ production of T cells *in vitro*. Strikingly, we found that $CD71^{+}$Neu but not $CD71^{-}$Neu acquired the ability to suppress both T cell proliferation and IFN-γ production in hypoxic conditions (**Fig. 4d**, **e**). Importantly, untreated or TES treated $CD71^{+}$Neu did not show suppressive abilities (**Fig. 4d**, **e** and **S4f, g**). Similarly to what observed *in vivo*, the potent suppressive ability of hypoxic $CD71^{+}$Neu correlated with a pro-tumoral signature characterized by the expression of *arg1* (**Fig. 4f**), *vegfa* and *tgfb* (**Fig. S4h**) by RT-qPCR. Of note, hypoxic $CD71^{-}$Neu and $CD71^{+}$Neu showed similar levels of HIF1α (**Fig. S4i**). We also confirmed an increased production of ARG-1 by hypoxic $CD71^{+}$Neu by WB (**Fig. 4g**), while no differences were observed in the inducible nitric

oxide synthetase (iNOS) expression (**Fig. S4j**). ARG-1 is a very a well-known suppressive marker expressed by immunosuppressive neutrophils. To assess ARG-1 contribution to the immunosuppressive capacity of hypoxic CD71$^+$Neu, we inhibited ARG-1 in the co-cultures of neutrophils with T cells using the arginine analogue norNOHA. Interestingly, we found that the treatment with norNOHA critically affected the ability of hypoxic CD71$^+$Neu to suppress the proliferation and the IFN-γ production of T cells (**Fig. 4h**), indicating that ARG-1 is a critical mediator of the suppressive ability of CD71$^+$Neu in hypoxic conditions. To confirm the relevance of this finding, we showed that also CD71$^+$Neu FACS sorted from SB28 tumors expressed higher levels of ARG-1 by WB compared to CD71$^-$Neu (**Fig. 4i**). Of note, neutrophils generated in hypoxic conditions from CD71 CKO mice showed a similar suppressive ability and ARG-1 levels of those generated from control mice, confirming that CD71 is not involved in the regulation of the suppressive ability of CD71$^+$Neu (**Fig. S4k, l, m**).

Altogether our data suggest that hypoxia is a major driver of the immunosuppressive ability of CD71$^+$Neu within GBM tumors through the induction of ARG-1 expression.

Hypoxia boosts glucose metabolism in CD71$^+$Neu.

Our scRNA-seq data indicated CD71$^+$Neu as a highly glycolytic sub-population of neutrophils. In addition, it is well established that hypoxia supports metabolic changes that may drive functional reprogramming of immune cells inside the TME[61]. Therefore, we asked whether hypoxia may drive metabolic changes in neutrophils. To understand the metabolic profile of neutrophils, we differentiated neutrophils in normoxic and hypoxic conditions with GM-CSF. At day 5, CD71$^-$Neu and CD71$^+$Neu were FACS sorted and assayed for their metabolic profile by Seahorse extracellular flux analyzer. Using Seahorse Mito Stress Test (**Fig. 5a-d**), we did non observe significant differences in the basal oxygen consumption rate (OCR) between CD71$^-$Neu and CD71$^+$Neu in normoxic and hypoxic condition (**Fig. 5a, c**). However, we found that CD71$^+$Neu, independently of hypoxia, showed higher spare respiratory capacity (SRC) (**Fig. S5a**). Importantly, normoxic CD71$^+$Neu showed higher basal extracellular acidification rate (ECAR) compared to

normoxic CD71$^-$Neu (**Fig. 5 b, d**). Hypoxic CD71$^+$Neu demonstrated even higher basal ECAR when compared with both normoxic CD71$^+$Neu and with normoxic and hypoxic CD71$^-$Neu (**Fig. 5 b, d**). These data suggested that CD71$^+$Neu have an intrinsic predisposition toward a glycolytic metabolism that is highly enhanced in hypoxic conditions. Thus, to further confirm that hypoxic CD71$^+$Neu are glycolytic cells, we analyzed their metabolic profile by Seahorse Glycolysis Stress Test (**Fig. 5e, f**). Our results confirmed that hypoxic CD71$^+$Neu showed higher glycolysis and glycolytic capacity than hypoxic CD71$^-$Neu and normoxic CD71$^-$Neu and CD71$^+$Neu (**Fig. 5f**). Altogether, these results validated the observations made with scRNA-seq analysis and further suggested that CD71$^-$Neu and CD71$^+$Neu are two distinct populations of neutrophils characterized by a different metabolic profile. CD71$^+$Neu are intrinsically more glycolytic than CD71$^-$Neu, and this glycolytic potential is enhanced in hypoxic conditions. This enhanced glycolytic profile of hypoxic CD71$^+$Neu was accompanied by a higher expression of both GLUT-1, a major receptor for the uptake of glucose, and LDHA, a rate-limiting enzyme for lactate production (**Fig. 5g**), similarly to what was reported in the scRNA-seq data. In line with that, hypoxic CD71$^+$Neu also showed increased levels of intracellular lactate (**Fig. 5h**). Collectively our data suggested that hypoxic CD71$^+$Neu are a highly glycolytic sub-population of Neu, accumulating massive amounts of intracellular lactate.

To verify the relevance of our *in vitro* data, we evaluated the ability of *in vivo* tumor associated neutrophils to uptake glucose using the fluorescent glucose tracer 2-(N-(7-nitrobenz-2-oxa-1,3-diazol-4-yl)amino)-2-deoxyglucose (2-NDGB) by flow cytometry. *In vivo* CD71$^+$Neu showed higher avidity to uptake 2-NDGB (**Fig. 5i**) and expressed higher levels of GLUT-1 compared to CD71$^+$Neu (**Fig. 5j**). Importantly, we also confirmed that CD71$^+$Neu expressed higher levels of LDHA (**Fig. 5k**), which was previously reported in the scRNA-seq as a distinctive marker of this population. To further confirm our scRNA-seq findings, tumor associated CD71$^+$Neu showed a higher expression of different glycolytic genes (**Fig. S5b**). Tumor associated CD71$^+$Neu also accumulated higher amounts of intracellular lactate (**Fig. 5l**).

To validate our data in human brain cancer patients, we analyzed glucose uptake and GLUT-1 expression by flow cytometry in tumor associated CD71$^-$Neu and CD71$^+$Neu. As observed in mouse tumors, human tumor associated CD71$^+$Neu demonstrated higher avidity for glucose (**Fig. 5m**) and higher GLUT-1 expression (**Fig. 5n**) than CD71$^-$Neu. In addition, also human CD71$^+$Neu showed a higher expression of different glycolytic genes (**Fig. S5c**), including *ldha* (**Fig. 5o**).

Since CD71$^+$Neu are immunosuppressive cells in both mouse and human brain tumors, our data indicated that glucose metabolism is associated and, therefore, could control the pro-tumoral functions of hypoxic CD71$^+$Neu.

Glycolysis and lactate govern the immunosuppressive activity of CD71$^+$Neu through histone lactylation.

It is well established that glucose and lactate can drive epigenetic and functional reprogramming of macrophages. In fact, an enhanced glycolysis and lactate production were shown to regulate the gene expression and immunosuppressive functions of macrophages by increasing lactylation levels of histones' lysine residues thus leading to an increased ARG-1 production[62-64]. Since our hypoxic CD71$^+$Neu showed increased glycolysis, lactate production and an ARG-1-dependent immunosuppressive activity, we analyzed histone lactylation (Kla) and acetylation (Kac) levels in both CD71$^-$Neu and CD71$^+$Neu, isolated from both *in vitro* cultures and directly from tumor tissue, using anti-Pan Kla and anti-Pan Kac[62] antibodies by WB. We found that both *in vitro* hypoxic CD71$^+$Neu (**Fig. 6a**) and *in vivo* tumor derived CD71$^+$Neu (**Fig. 6b**) demonstrated higher Kla levels compared to *in vitro* hypoxic CD71$^-$Neu, normoxic CD71$^-$Neu and CD71$^+$Neu and *in vivo* CD71$^-$Neu, respectively. Importantly, no differences in Kac levels were observed in both *in vitro* and *in vivo* neutrophils (**Fig. 6a, b**). Similarly to what was previously reported for macrophages, also in hypoxic and in tumor derived CD71$^+$Neu high levels of Kla correlated with an higher *arg1* transcription and synthesis. Thus, to test if Kla can regulate *arg1* transcription in tumor derived CD71$^+$Neu, we analyzed the Kla marks at the promoters of *arg1* gene, using CUT&RUN assay with an anti-Pan Kla

antibody followed by qPCR, which was optimized in our laboratory. CUT&RUN assay confirmed that CD71^{+}Neu showed higher levels of Kla marks at the promoter regions of *arg1* compared to CD71^{-}Neu (**Fig. 6c**). Collectively, our data suggest that glucose-driven histone lactylation in CD71^{+}Neu may play a detrimental role in the reprogramming of CD71^{+}Neu towards cells with potent immunosuppressive activity.

Next, to assess the contribution of glycolysis and lactate to the immunosuppressive activity of CD71^{+}Neu, we analyzed the suppressive function of *in vitro* hypoxic Neu treated with 2-deoxyglucose (2-DG), a glycolysis inhibitor, and GNE-140, an inhibitor of lactate dehydrogenase[62]. Strikingly, both the treatment with 2-DG (**Fig. 6d**) and GNE-140 (**Fig. 6e**) hampered the capacity of hypoxic CD71^{+}Neu to suppress the proliferation and IFN-γ production of CD4^{+} and CD8^{+} T cells. In addition, 2-DG and GNE-140 treatments drastically suppressed the transcription (**Fig. 6f, g**) and synthesis (**Fig. 6h**) of ARG-1. The reduced ARG-1 expression that followed the inhibition of glycolysis and LDH was associated with a simultaneous reduction of the Kla levels (**Fig. 6i**). Furthermore, we performed CUT&RUN assay on hypoxic CD71^{+}Neu treated with either 2-DG or GNE-140. CUT&RUN assay first confirmed that hypoxic CD71^{+}Neu showed higher levels of Kla marks at the promoter regions of *arg-1* compared to hypoxic CD71^{-}Neu (**Fig. 6j**). Moreover, 2-DG and GNE-140 treatments were able to drastically reduce the levels of Kla marks at the promoter regions of *arg1* in hypoxic CD71^{+}Neu (**Fig. 6j**), confirming the detrimental role of both the glycolysis and lactate in controlling Kla levels and, subsequently, ARG-1 expression in hypoxic CD71^{+}Neu. To assess the contribution of GLUT-1 to the suppressive activity of CD71^{+}Neu, we created myeloid-specific conditional mice deficient in Slc2a1 (GLUT-1) by crossing a Slc2a1$^{fl/fl}$ mouse with a Ly2z Cre^{+} mouse (Slc2a1$^{fl/fl}$ Cre^{+}). CD71^{+}Neu isolated from brain tumors (SB28) orthotopically established in Slc2a1$^{fl/fl}$ Cre^{+} mice, exhibited a very low expression of GLUT-1 (**Fig. S6a**) and an impaired ability to suppress the proliferation of both CD4^{+} and CD8^{+} T cells (**Fig. 6k**).

Finally, since also Kac levels can control ARG-1 expression in different ways, depending on the immune cell type[65-70], and in different cells, including MDSC[71], we assessed the

contribution of Kac to the immunosuppressive phenotype of hypoxic CD71$^+$Neu, by treating *in vitro* hypoxic Neu with BMS-303141, an inhibitor of the acetyl-CoA production, able to inhibit Kac[72]. Importantly, Kac do not hampered the immunosuppressive activity and the ARG-1 expression of hypoxic CD71$^+$Neu (**Fig. S6b, c, d**). These results, together with those showing no differences in the Kac levels between CD71$^+$Neu and CD71$^-$Neu both *in vitro* and *in vivo*, confirmed the exclusive role of Kla in controlling the immunosuppressive reprogramming of hypoxic and tumor associated CD71$^+$Neu.

Collectively, these results demonstrate that the increased glycolysis and lactate production observed in both *in vitro* hypoxic CD71$^+$Neu and *in vivo* tumor associated CD71$^+$Neu, induce high levels of Kla at the *arg1* promoter, promoting an increased ARG-1 synthesis and thus reprogramming CD71$^+$Neu phenotype towards highly immunosuppressive cells.

CD71$^+$Neu are mobilized from BM during tumor progression and persist longer within the TME.

Our previous data showed that CD71$^+$Neu progressively infiltrate GBM tumors during tumor progression, being mostly expanded inside the tumor at later stages. Thus, we investigated the possible reasons behind this higher accumulation of CD71$^+$Neu in later stages of brain tumors compared to earlier stages and to the periphery. One possible explanation could be that neutrophils migrate inside brain tumors and there upregulate the CD71 receptor. However, our data suggested that CD71$^-$Neu and CD71$^+$Neu are two distinct population. Moreover, the results showed in figure S4 indicated that both human and mouse neutrophils are not able to upregulate the CD71 when exposed to either hypoxia or tumor derived factors. Also, in the figure S3c we showed no differences in the frequency of CD71$^+$Neu in the BM or spleen of brain tumor-bearing mice compared to tumor-free mice, indicating that there is not an increase in CD71$^+$Neu production in the BM or spleen during tumor progression. However, when we looked at the frequencies in the blood, we observed a drastic increase throughout tumor progression of both the total neutrophils population and, to a larger extent, of CD71$^+$Neu in both the GL261 and SB28 models (**Fig. 7a, b**). The same result was obtained when looking at CD71$^+$Neu frequencies

in the blood of healthy donors vs brain cancer patients (**Fig. 7c**). Neutrophilia and the recruitment in the circulation of immature neutrophils occur in both humans and mice and can promote immunosuppression[17,73,74]. Thus, our results together with the literature, suggested an increase in total neutrophils and, more specifically, in CD71^{+}Neu mobilization from the BM during tumor progression and prompted us to look at the chemokines receptors in BM derived neutrophils. neutrophils trafficking from BM into peripheral blood is tightly regulated, particularly by signaling through the chemokine receptors CXC-chemokine receptor 2 and 4 (CXCR2 and CXCR4). Expression of CXC-chemokine ligand 12 (CXCL12) by bone marrow stromal cells mediates the retention of CXCR4^{+} immature neutrophils. Downregulation of CXCR4 coupled with the upregulation of CXCR2 and the activation of its signaling in BM neutrophils, triggers the entry of neutrophils into the peripheral blood. Thus, in the circulation, neutrophils newly released from the bone marrow are characterized by high expression of CXCR2 and low expression of CXCR4[15]. Moreover, the upregulation of CXCR4 in tumor associated neutrophils is associated with aged and pro-tumoral neutrophils, capable of promoting tumor growth and metastasis[75,76]. Compared to BM neutrophils from tumor-free mice, both BM CD71^{-}Neu and CD71^{+}Neu from SB28-bearing mice significantly upregulated CXCR2 (**Fig. 7d**), supporting the increased recruitment of neutrophils in the circulation observed in SB28-bearing mice. CXCR4 expression was not significantly modulated in both the BM population (**Fig. S7a, b**). Of note, compared to their naïve counterpart, CD71^{+}Neu upregulated CXCR2 significantly more than CD71^{-}Neu (**Fig. 7d** and **S7b**), indicating a higher mobilization of this population during tumor progression that could, at least partially, explain their expansion inside brain tumors at later stages. When comparing blood CD71^{-}Neu and CD71^{+}Neu from SB28-bearing mice, no differences were observed in the expression of both CXCR2 and CXCR4 (**Fig. S7c, d, e**). However, tumor associated CD71^{+}Neu expressed similar levels of CXCR2 (**Fig. 7e**) and significantly higher levels of CXCR4 (**Fig. 7f**) when compared to tumor associated CD71^{-}Neu (**Fig. S7e**). The similar levels of CXCR2 indicated that probably the recruitment rate to the tumor site is similar between the two populations of neutrophils. However, the increased CXCR4 expression

by tumor associated CD71^{+}Neu[75,76], together with their increased GLUT-1 expression[77], suggested that CD71^{+}Neu may be aged neutrophils that are capable of persisting longer within the tumor bed, acquiring pro-tumoral features. To confirm this, we injected bromodeoxyuridine (BrdU) in SB28-bearing mice. BrdU is an analog of the DNA precursor thymidine that is incorporated into newly synthesized DNA by proliferating cells and persists in the cells until their death or until it gets diluted and lost following several cell divisions[78]. BrdU incorporation can be detected by flow cytometry using fluorochromes associated anti-BrdU antibodies. If measured few hours after the administration, BrdU incorporation can be used to quantify the *in vivo* proliferation potential of the cells. In addition, by studying the persistence of BrdU^{+} cells several days after BrdU administration, it can reveal information regarding the turnover and the age of cells *in vivo*[77]. 3 hours post injection, CD71^{+}Neu showed a slightly, but not significantly, higher BrdU incorporation compared to CD71^{-}Neu in the periphery; however, their proliferation ability was strongly increased inside the tumor, compared to both the periphery and tumor associated CD71^{-}Neu (**Fig. 7g**), indicating that these cells most likely acquire proliferation abilities inside the TME. Between day 2 and 4, BrdU^{+}Neu reached their peak in both the periphery and the tumor (data not shown), indicating that neutrophils quickly colonize both the peripheral organs and the tumor, as previously reported[77]. 9 days after BrdU administration, almost all neutrophils in the periphery were BrdU^{-} and, thus, had been replaced by younger neutrophils (**Fig. 7h**). However, at the tumor site, almost 30% of CD71^{+}Neu were still BrdU^{+} and, thus, 9 days old, while most of CD71^{-}Neu were BrdU^{-}, indicating that, differently from CD71^{+}Neu, most of CD71^{-}Neu coming from day 0 had been replaced by younger cells (**Fig. 7h**). These data suggested that CD71^{+}Neu can proliferate and persist longer inside the GBM TME compared to CD71^{-}Neu. This appears in line with our previous findings reporting that tumor associated CD71^{+}Neu expressed more CD117, as the proliferating neutrophils recently described[55], and more GLUT-1 and CXCR4, as the aged and long-persisting pro-tumoral neutrophils reported in the literature[75-77]. This seems also coherent with the role of CD71 that was described as an important receptor to sustain the proliferation of different cells[55,79]. However, CD71 was

also described as capable of inducing ferroptosis and, thus, cell death in different cell types[80], contrasting our previous results that showed how CD71$^+$Neu can persist longer inside the GBM TME. Therefore, we decided to stain SB28 tumors with LiperFluo, a routinely used method to assess the accumulation of lipid peroxide in the cells and, thus, able to indirectly measure the amount of ferroptosis[81]. Surprisingly, CD71$^+$Neu did not accumulate lipid peroxide in GBM tumors (**Fig. 7i**). In line with that, tumor associated CD71$^+$Neu showed higher levels of the Glutathione Peroxidase 4 (GPX4) (**Fig. 7j**), the main inhibitor of lipid peroxidation and, thus, of ferroptosis[82]. In line with that, hypoxia increased the levels of GPX4 in CD71$^+$Neu while decreasing them in CD71$^-$Neu (**Fig. 7k**), conferring a survival advantage to hypoxic CD71$^+$Neu (**Fig. 7l**).

Altogether, our results suggest that during GBM progression CD71$^+$Neu are highly mobilized from the BM; when they reach the GBM TME, CD71$^+$Neu acquire a proliferative potential and resistance to ferroptosis, thus being able to persist longer at the tumor site.

LDHA targeting through IFNα and Isosafrole prolonged the survival of GBM bearing mice.

Our data showed that neutrophils play a central role in favoring brain cancer progression, through the suppression of T cells functions. In particular, the glycolytic population of CD71$^+$Neu was the key contributor to this immunosuppressive activity. Hypoxia-driven lactate accumulation and increased Kla levels were able to shape CD71$^+$Neu function, controlling their pro-tumoral activity. Thus, we reasoned that targeting LDHA *in vivo* could result in a reduced lactate production and Kla levels in tumor associated CD71$^+$Neu, with a consequent loss of their immunosuppressive functions leading to a reduced tumor progression. Based on a recent publication showing that Interferon α (IFNα) can shape tumor cells glycolytic metabolism and reduce LDHA levels and activity[83], we decided to first test the potential of IFNα in our *in vitro* model. IFNα treatment was able to reduce LDHA expression in hypoxic CD71$^+$Neu and, consequently, reduced the levels of intracellular lactate and Kla, with a consequent loss of ARG-1 expression (**Fig. 8a** and **S8a, b**) and a complete abrogation of hypoxic CD71$^+$Neu immunosuppressive ability (**Fig. 8b,**

c). Thus, we decided to test the efficacy of IFNα directly *in vivo* in SB28-bearing mice. Starting from day 7 after the intra-cranial tumor challenging, we intraperitoneally injected 10,000 I.U./mouse of IFNα every day. The treatment with IFNα strongly improved the survival of SB28-bearing mice (**Fig. 8d**).

In addition, we revised the literature and found that the anti-epileptic drug stiripentol was able to efficiently cross the blood-brain barrier to inhibit LDHA/B activity in the brain of mice[84] and successfully slowed tumor progression in a pre-clinical model of murine brain tumor[85]. Interestingly, another work showed that an analog of stiripentol, isosafrole, inhibited LDH enzymes and lactate production to a larger extent than stiripentol, thus potently suppressing lactate-dependent seizures *in vivo* in murine models[84]. However, its potential in GBM models was never investigated. Therefore, we first tested the effects of isosafrole treatment in our *in vitro* system. Compared to the control, isosafrole strongly reduced LDHA, intracellular lactate and Kla levels, completely abrogating ARG-1 production and the immunosuppressive activity of hypoxic $CD71^{+}$Neu (**Fig. 8e, f, g** and **S8c, d**). Giving the promising results obtained *in vitro*, we tested isosafrole also *in vivo*. Starting 7 days after the tumor cells challenging, we treated SB28-bearing mice intraperitoneally with a dose of 200 mg/kg of isosafrole, every other day. Strikingly, the treatment with isosafrole drastically delayed tumor growth in SB28-bearing mice (**Fig. 8h**).

Collectively, our data demonstrate the potential of targeting LDHA and lactate production in brain tumors. In particular, the repurposing of IFNα and of the anti-epileptic drug isosafrole, both of which showed a potent ability in reducing $CD71^{+}$Neu immunosuppression, for the treatment of GBM-bearing mice, resulted in a dramatic effect in delaying tumor growth. Thus, these pre-clinical results highlight the promising potential of introducing these drugs also in novel therapeutical approaches for human GBM patients.

Discussion

Glioblastoma is characterized by a profound immunosuppressive TME that restricts the success of promising immunotherapies. Neutrophils recently emerged as key contributors to the GBM immunosuppressive TME[19,23,27,86-88]. However, the mechanisms by which neutrophils govern the immunosuppressive state of GBM tumors remained unknown[9]. With this paper, we functionally characterized for the first time tumor associated neutrophils in the context of murine and human brain tumors. As previously reported[26], we confirmed that Neu depletion had a critical effect in prolonging the survival of GBM-bearing mice. This was largely due to their ability of suppressing T cells responses, as neutrophils' depletion resulted in a dramatic expansion in T cells infiltration. Similarly, neutrophils infiltration in human brain cancer was inversely correlated with T cells infiltration. These data strengthen the concept that neutrophils accumulation in GBM TME is a critical factor in limiting the success of immunotherapies[27].

Single-cell RNA sequencing analysis in blood versus tumor derived neutrophils allowed us to probe neutrophils heterogeneity in the SB28 murine model of GBM. It is well established that different subsets of neutrophils can coexist in the same cancer patient[16,34,36-38,89,90]. Pro-tumoral and immunosuppressive neutrophils are usually referred as PMN-MDSC[91], however it is still not clear if PMN-MDSC represent a unique population of neutrophils or if they just represent a functional state induced by the tumor. Moreover, no unique markers able to precisely discriminate between pro-tumoral and classical neutrophils in both mice and humans have been described so far. Finally, in most of the studies available at this moment in brain tumors, neutrophils have been considered as a homogeneous population and referred as either neutrophils or PMN-MDSC, limiting the relevance of the findings. Our scRNA-seq analysis showed that blood neutrophils reach the GBM TME where they are reprogrammed, forming 9 main clusters. Interestingly, a high glycolytic subset of neutrophils was largely expanded inside the tumor, showing an increased hypoxic signature and other features previously associated with immunosuppressive neutrophils. A glycolytic population of Neu showing pro-tumoral

function was recently identified also in the context of pancreatic ductal adenocarcinoma (PDAC)[92]. However, no surface markers were identified in order to easily distinguish this population of neutrophils and an in-depth characterization of how the TME controlled and reprogrammed these cells was lacking. Similarly to what was observed in PDAC, also our population of glycolytic Neu expressed high levels of LDHA. However, LDHA is not uniquely expressed by this subset of neutrophils. Interestingly, our scRNA-seq revealed that glycolytic Neu were characterized by the exclusive expression of CD71. Consequently, flow cytometry staining allowed the identification of 2 different sub-populations of neutrophils in both murine and human brain tumors, based on the expression of CD71: $CD71^{-}$Neu and $CD71^{+}$Neu. $CD71^{+}$Neu were expanded within the TME compared to the periphery. Contrary to $CD71^{-}$Neu, only $CD71^{+}$Neu acquired pro-tumoral features and a strong immunosuppressive ability at the tumor site.

A proliferating early unipotent neutrophil progenitor population characterized by the coexpression of CD71 and CD117 was recently identified in the human bone marrow[55]. These cells were expanded in the blood of melanoma patients and detectable in blood and tumors from lung cancer patients. Our tumor associated $CD71^{+}$Neu expressed high levels of CD117 and a higher proliferating potential compared to $CD71^{-}$Neu. However, they showed a mature morphology, higher levels of LY6G, CD101 and CD11B, suggesting common features with both mature and immature cells. This may suggest that once $CD71^{+}$Neu migrate into the TME, they undergo maturation and activation without losing the expression of CD71 and CD117. In support of this hypothesis, our *in vitro* model showed that hypoxia is able to induce maturation and upregulation of both LY6G and CD11B in $CD71^{+}$Neu. Overall, GBM is one of the most hypoxic tumor types[53,54], with an intratumoral average of 1.25% O_2 levels[93]. This, together with our scRNA-seq data showing that most of SB28 tumor associated Neu are exposed to a strongly hypoxic TME, support the relevance of our *in vitro* model based on 1% O_2 cultures.

Hypoxia induced an ARG-1-dependent immunosuppressive activity selectively in $CD71^{+}$Neu. These results are in line with a previous publication showing that hypoxia is

able to control the differentiation and function of MDSC[94]. Moreover, ARG-1 was already linked with the ability of neutrophils to suppress T cells in GBM[33]. However, molecular insights showing how hypoxia can reprogram immunosuppressive neutrophils were missing. Moreover, clear evidence of how neutrophils metabolism can drive their function within the TME were never reported. We found that, differently from CD71$^-$Neu, CD71$^+$Neu have an intrinsic predisposition toward a glycolytic metabolism that is highly enhanced in hypoxic conditions, together with an increased LDHA expression. This difference in their metabolism, leads CD71$^+$Neu to produce and accumulate higher levels of intracellular lactate both *in vitro* under hypoxic conditions and *in vivo* within the TME. A recent study demonstrated that glucose is incompletely oxidized to produce the metabolite lactate which generate lactyl-CoA[62]. This lactyl-CoA acted to add a lactyl group to the lysine tails of histone proteins to produce a modification called histone lactylation[62]. Histone lactylation (Kla) promotes the expression of homeostatic genes in the late phase of *in vitro* polarization with LPS/IFN-γ[62] as well as reparative genes in macrophages that regulate inflammation resolution and cardiac repair initiation after myocardial infarction[63]. Moreover, Kla was able to reprogram immunosuppressive M2-like macrophages by controlling ARG-1 expression[62,64]. However, the role of Kla in neutrophils was never investigated. We found that both *in vitro* hypoxic CD71$^+$Neu and *in vivo* tumor associated CD71$^+$Neu had increased levels of Kla. CUT&RUN assay confirmed higher level of Kla marks at the *ARG-1* promoter in CD71$^+$Neu, supporting the idea that, similarly to what was observed in macrophages[62,64], Kla can control ARG-1 expression also in hypoxic CD71$^+$Neu. Inhibiting glycolysis through 2-DG and lactate production through the LDHA inhibitor GNE-140, led to a dramatic reduction in Kla and ARG-1 levels, and a complete abrogation of the immunosuppressive ability of hypoxic CD71$^+$Neu, confirming the detrimental role of glycolysis and lactate production in reprogramming the function of these cells. Some papers showed that also Kac levels can control ARG-1 synthesis in different and opposite ways depending on the immune cell type[65-70], including MDSC[71]. However, both *in vitro* hypoxic CD71$^+$Neu and *in vivo* tumor associated CD71$^+$Neu did not show changes in Kac levels compared to both CD71$^-$Neu and to their normoxic

counterpart. Moreover, inhibition of Kac did not reduce ARG-1 expression and did not alter the immunosuppressive activity of hypoxic Neu, indicating that Kac levels are not involved in the immunosuppressive reprogramming of hypoxic CD71^{+}Neu.

CD71^{+}Neu were expanded in the blood and tumor of both GBM-bearing mice and GBM human patients. CD71 expression could not be induced in either murine or human CD71^{-} Neu. In addition, CD71^{+}Neu were not expanded in both the spleen and BM of GBM-bearing mice, suggesting that their production is not increased during tumor progression. Our scRNA-seq data suggested that blood neutrophils are recruited inside the tumor. Our cytokines receptors staining suggested that both CD71^{-}Neu and CD71^{+}Neu are highly mobilized from the BM during tumor progression. However, compared to their naïve counterpart, BM CD71^{+}Neu upregulated the CXCR2 receptor to a larger extent compared to CD71^{-}Neu, thus explaining their massive expansion throughout tumor progression in the blood of both murine GBM models and human patients. Previous studies already highlighted how the expansion of neutrophils in the circulation and the massive recruitment of immature cells promote immunosuppression in both mice and humans[17,73,74]. Neutrophils trafficking from BM into the circulation is finely controlled by signaling through the chemokine receptors CXCR2 and CXCR4. Expression of CXCL12 by BM stromal cells retains CXCR4^{+} immature neutrophils inside the BM. Downregulation of CXCR4 together with upregulation of CXCR2 and activation of its signaling in BM neutrophils, triggers the entry of neutrophils into the peripheral blood. CXCR2 levels on neutrophils surface tightly regulate their recruitment at the tumor site[95]. The similar expression of CXCR2 by CD71^{-}Neu and CD71^{+}Neu in both blood and tumor of SB28-bearing mice, suggested a similar recruitment rate of both these two neutrophils populations at the tumor site. Thus, a higher mobilization from BM could only partially explain the observed expansion of CD71^{+}Neu at the tumor site. However, the increased expression of GLUT-1 and CXCR4 by tumor associated CD71^{+}Neu suggested an increased persistency of these cells within the tumor microenvironment, as the increased expression of both these receptors at the tumor site was previously associated with aged and pro-tumoral Neu[75-77]. The high CD117 and CD71 expression by tumor CD71^{+}Neu also

suggested that these cells could exhibit proliferating abilities[55]. BrdU experiments confirmed that CD71^{+}Neu show an increased proliferating potential within the tumor and are able to persist longer inside GBMs compared to CD71^{-}Neu. Since CD71 is a marker of ferroptotic cells[80], we would have expected an increased susceptibility of these cells to undergo ferroptosis at the tumor site. Strikingly, LiperFluo staining indicated a reduced accumulation of peroxides lipids by these cells at the tumor site, accompanied by a dramatic upregulation of GPX4, the main inhibitor of ferroptosis[82]. Hypoxia was able to upregulate GPX4 expression in CD71^{+}Neu while reducing it in CD71^{-}Neu, conferring a survival advantage to hypoxic CD71^{+}Neu. These results are in line with a recent paper in which LY6G^{high} neutrophils isolated from the BM (mostly CD71^{-}, as previously reported in our results) downregulated GPX4 when exposed to hypoxia[96]. Contrary to what was reported in this paper, our CD71^{+}Neu seems to upregulate GPX4 in hypoxic conditions as a compensatory mechanism allowing them to persist longer in the TME and suppress T cells responses. However, the differences observed in these 2 diverse systems suggest an intricate link between hypoxia, glucose metabolism, GPX4 expression, ferroptosis regulation and CD71^{+}Neu functions, which will need to be further investigated in future studies.

Finally, since neutrophils played a pivotal role in determining the survival of GBM-bearing mice and since their immunosuppressive ability relied on lactate-dependent Kla, we decided to target LDHA *in vivo* with the aim of reducing lactate accumulation and KLA in CD71^{+}Neu, thus hampering their immunosuppressive ability. Importantly, LDHA targeting has recently emerged as a very promising approach to treat cancer patients[97]. In fact, individuals showing genetic deficiencies in LDHA subunits only develop minor symptoms as muscle rigidity and myoglobinuria after strenuous excercise[98,99], thus indicating potential high anticancer efficacy, accompanied by only minor side effects. We developed 2 different therapeutical approaches to target LDHA in a murine GBM model, involving either IFNα or the anti-epileptic drug Isosafrole. Both the drugs already showed their great potential in efficiently targeting LDHA[83,84] and revealed able to completely hamper the immunosuppressive ability of *in vitro* hypoxic CD71^{+}Neu through the

reduction of Kla levels and the subsequent inhibition of ARG-1 production. When administered to SB28-bearing mice, both the compound showed a dramatic effect in prolonging mice survival, suggesting their promising role as anti-GBM treatments. Of note, IFNα already showed promising results in a phase 3 randomized trial for the treatment of newly diagnosed high-grade gliomas in combination with temozolomide[100].

In summary, our study probed for the first time neutrophils heterogeneity in the context of brain tumors. We identified the glycolytic population of CD71$^+$Neu as able of strongly suppress T cells function in both human and mice brain tumors. CD71$^+$Neu reach GBM tumors where they are reprogrammed by the hypoxic TME, becoming able to persist longer within the tumor, thanks to their proliferating ability and resistance to ferroptosis, and acquiring immunosuppressive features. CD71$^+$Neu are cells with an intrinsic predisposition towards a glycolytic metabolism, which is strongly increased in hypoxic conditions, leading to increased intracellular lactate levels, Kla levels and ARG-1 production. Due to the incomplete understanding of the mechanisms by which neutrophils can shape the immunosuppressive TME, targeting pro-tumoral neutrophils has so far proven to be extremely difficult[40,41]. However, our study presented an in-depth characterization of how the glycolytic metabolism is able to shape the function of immunosuppressive CD71$^+$Neu within the hypoxic GBM TME. So, we were able to target this novel mechanism by inhibiting LDHA *in vivo*, using IFNα and Isosafrole, and thus proposing these two drugs as very promising compounds to be introduced in future therapeutical approaches for patients with brain cancer.

Figures

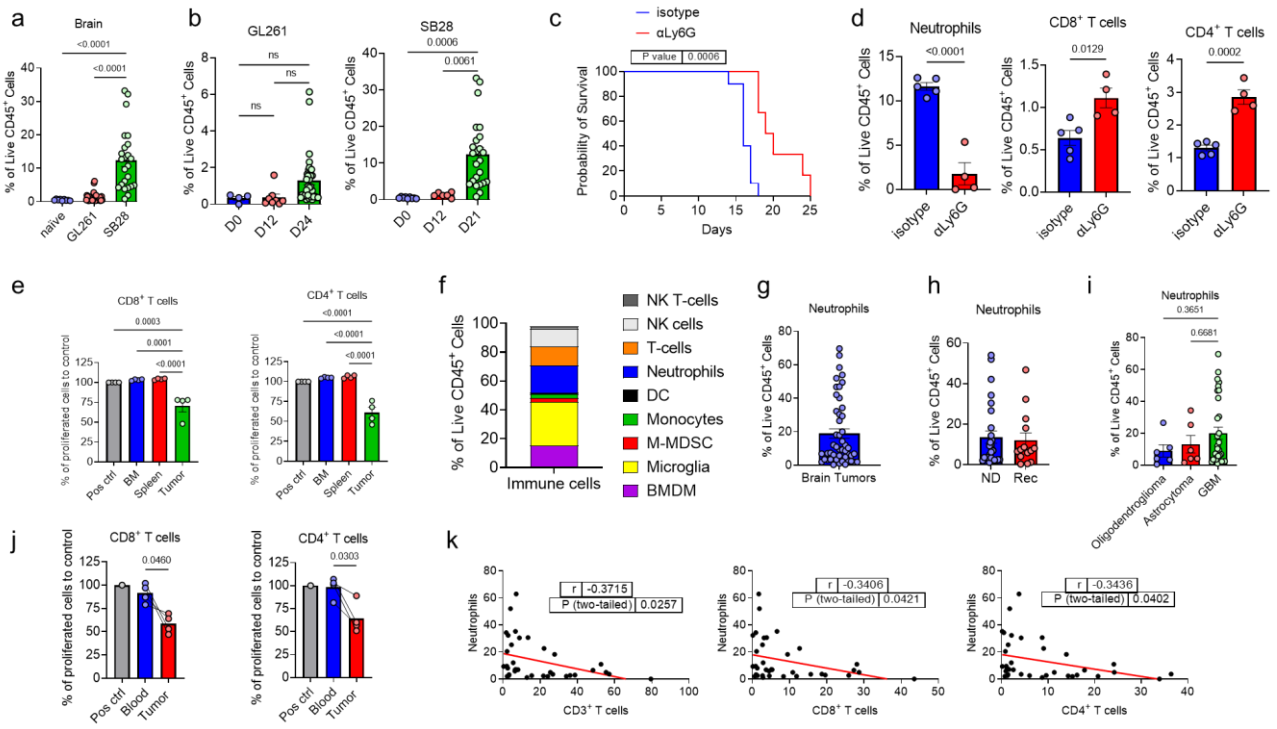

Fig. 1 - Neutrophils infiltrate brain tumors acquiring immunosuppressive features.

(**a**). Frequency of Neu out of live CD45⁺ cells in the brain of naive vs GBM-bearing mice by FACS. (**b**). Frequency of Neu out of live CD45⁺ cells in GL261 vs SB28 GBM murine models by FACS. (**c**). Kaplan-Meier representation of SB28-bearing mice treated with the isotype control or the Neu depleting strategy (αLy6G). (**d**). Frequency of Neu, CD8⁺ and CD4⁺ T cells out of live CD45⁺ cells in tumor of SB28-bearing mice after Neu depletion by FACS. (**e**). Suppressive ability of mouse tumor (SB28) derived Neu on CD8⁺ and CD4⁺ T cells proliferation, measured as CFSE dilution by FACS. (**f**). Frequencies of different immune cells out of live CD45⁺ cells in brain cancer patients from Moffitt Cancer Center (USA) and Policlinico Umberto I by FACS. (**g**). Frequency of Neu out of live CD45⁺ cells in brain cancer patients from Moffitt Cancer Center (USA) and Policlinico Umberto I by FACS. (**h**). Frequency of Neu out of live CD45⁺ cells in brain cancer patients divided in newly diagnosed (ND) and recurrent (Rec) from Moffitt Cancer Center (USA) and Policlinico Umberto I by FACS. (**i**). Frequency of Neu out of live CD45⁺ cells in brain cancer patients divided based on the diagnosis from Moffitt Cancer Center (USA) and Policlinico Umberto I by FACS. (**j**). Suppressive ability of human tumor derived Neu on CD8⁺ and CD4⁺ T cells proliferation, measured as CFSE dilution by FACS. (**k**). Correlation between the presence of Neu and T cells in the tumor of brain cancer patients by FACS. All data are presented as mean ± SEM. Statistical analysis was performed using one-way ANOVA with Tukey's post hoc test (**a**, **b**, **e** and **i**), Kaplan-Meier method and log-rank test (**c**), unpaired two-sided Student's *t*-tests (**d** and **h**), paired two-sided Student's *t*-tests (**j**) and Pearson Correlation Coefficient with the associated two-tailed *p* value (**k**).

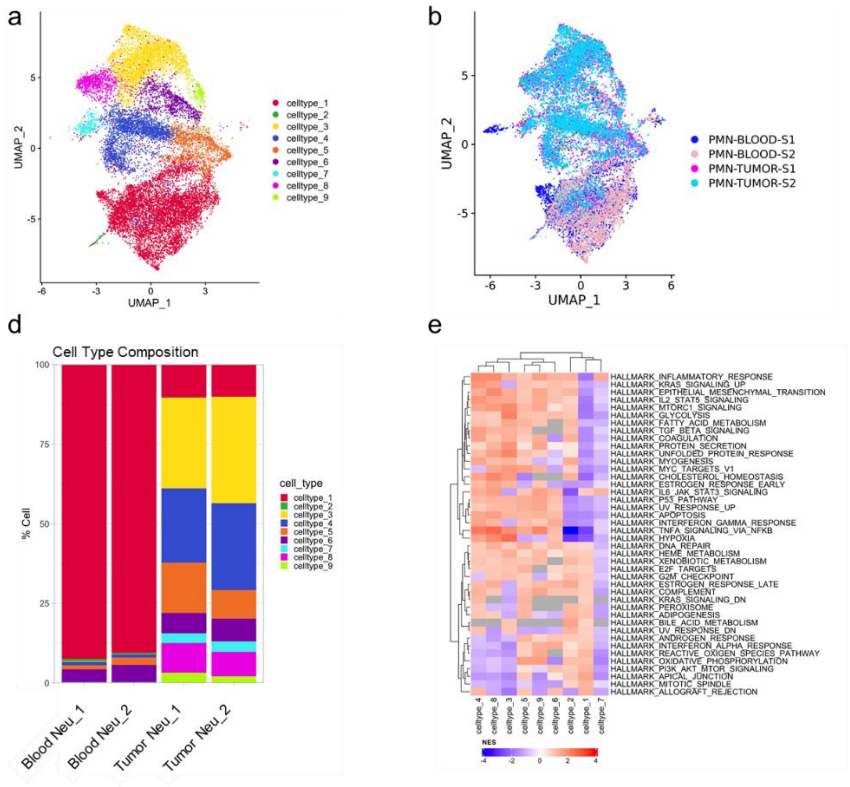

c

cell type	markers	annotation
celltype_1	Lyz2+Rac2+	Conventional
celltype_2	Adpgk+Camp+	Metabolic
celltype_3	Ldha+Tfrc+	Glycolytic
celltype_4	Cxcl3+Fpr1+	Inflamation
celltype_5	Bcl2l15+	
celltype_6	Ifit+	Interferon response
celltype_7	LowCount	
celltype_8	Eif5a+Atf3+	Stress response
celltype_9	Cd63+Ccrl2+	Activated

Fig. 2 - A population of glycolytic neutrophils expressing the CD71 receptor is expanded in brain tumors where it acquires a hypoxic signature.

(**a**). Unsupervised clustering of Neu. (**b**). Unsupervised clustering of Neu based on sample's origin. (**c**). Main features of the different Neu clusters. (**d**). Cell type composition of the different samples. (**e**). Pathway analysis in the different Neu clusters.

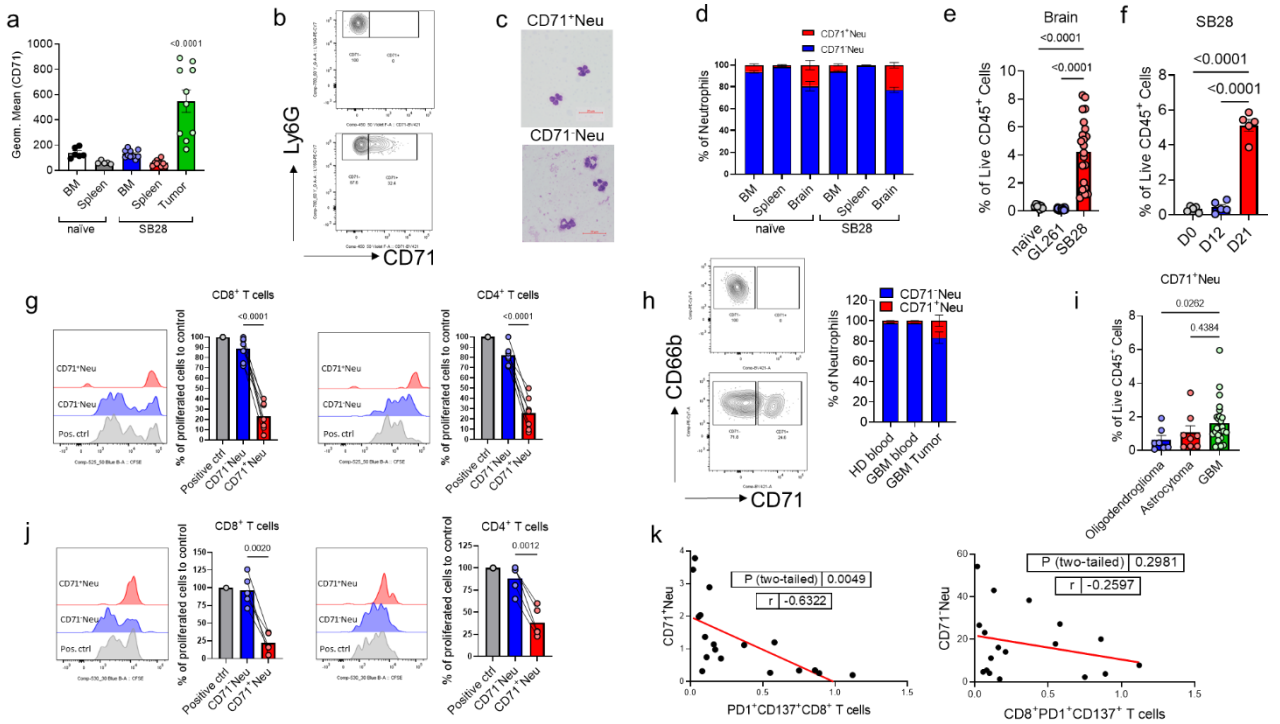

Fig. 3 - CD71⁺Neu are critical contributors to the immunosuppressive activity associated with neutrophils in brain tumors.

(**a**). CD71 expression in different murine organs by FACS. (**b**). Example of murine tumor derived Neu gating strategy based on CD71 expression by FACS. (**c**). Giemsa staining of tumor derived Neu. (**d**). Frequencies of CD71⁺Neu and CD71⁻Neu in different murine organs by FACS. (**e**). Frequency of CD71⁺Neu out of live CD45⁺ cells in murine brain by FACS. (**f**). Frequency of CD71⁺Neu out of live CD45⁺ cells in the SB28 GBM murine model over time by FACS. (**g**). Suppressive ability of mouse tumor (SB28) derived CD71⁺Neu and CD71⁻Neu on CD8⁺ and CD4⁺ T cells proliferation, measured as CFSE dilution by FACS. (**h**). Example of human tumor derived Neu gating strategy based on CD71 expression (left) and frequencies of CD71⁺Neu and CD71⁻Neu in human blood and tumor (right), by FACS. (**i**). Frequency of CD71⁺Neu out of live CD45⁺ cells in human brain cancers. (**j**). Suppressive ability of human tumor derived CD71⁺Neu and CD71⁻Neu on CD8⁺ and CD4⁺ T cells proliferation, measured as CFSE dilution by FACS. (**k**). Correlation between the presence of CD71⁺Neu or CD71⁻Neu and PD1⁺CD137⁺CD8⁺ T cells in the tumor of brain cancer patients by FACS. All data are presented as mean ± SEM. Statistical analysis was performed using one-way ANOVA with Tukey's post hoc test (**a**, **e**, **f** and **i**), paired two-sided Student's *t*-tests (**g** and **j**) and Pearson Correlation Coefficient with the associated two-tailed *p* value (**k**).

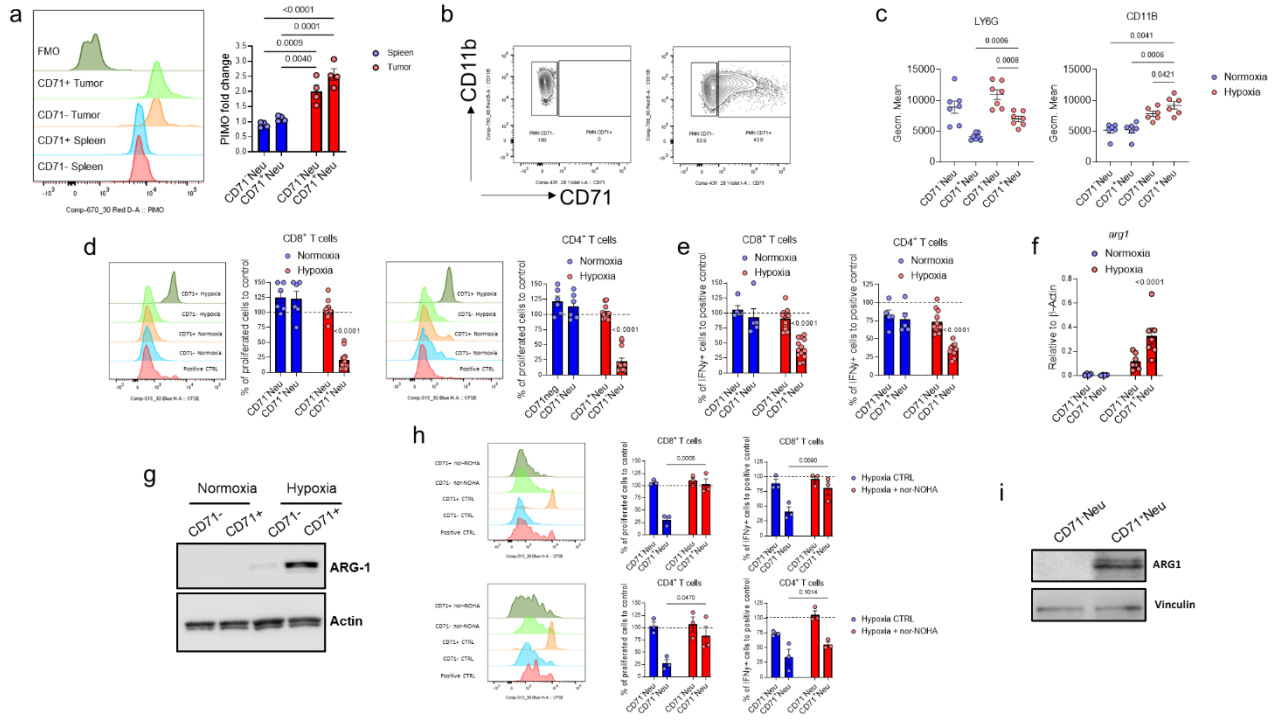

Fig. 4 - Hypoxia drives immunosuppressive function and ARG-1 expression in CD71⁺Neu.

(**a**). anti-PIMO staining by FACS, expressed as PIMO Geom. Mean fold change to splenic Neu. (**b**). Example of murine *in vitro* Neu gating strategy based on CD71 expression by FACS. (**c**). LY6G and CD11B expression in *in vitro* Neu by FACS. (**d**). Suppressive ability of *in vitro* CD71⁺Neu and CD71⁻Neu on CD8⁺ and CD4⁺ T cells proliferation, measured as CFSE dilution by FACS. (**e**). Suppressive ability of *in vitro* CD71⁺Neu and CD71⁻Neu on CD8⁺ and CD4⁺ T cells IFN-γ production by FACS. (**f**). *arg1* expression by RT-QPCR in *in vitro* Neu. (**g**). WB of indicated markers in *in vitro* Neu. (**h**). Suppressive ability of *in vitro* CD71⁺Neu and CD71⁻Neu treated with nor-NOHA on CD8⁺ and CD4⁺ T cells proliferation (left), measured as CFSE dilution, and IFN-γ production (right), by FACS. (**i**). WB of indicated markers in tumor derived Neu. All data are presented as mean ± SEM. Statistical analysis was performed using two-way ANOVA with Tukey's post hoc test.

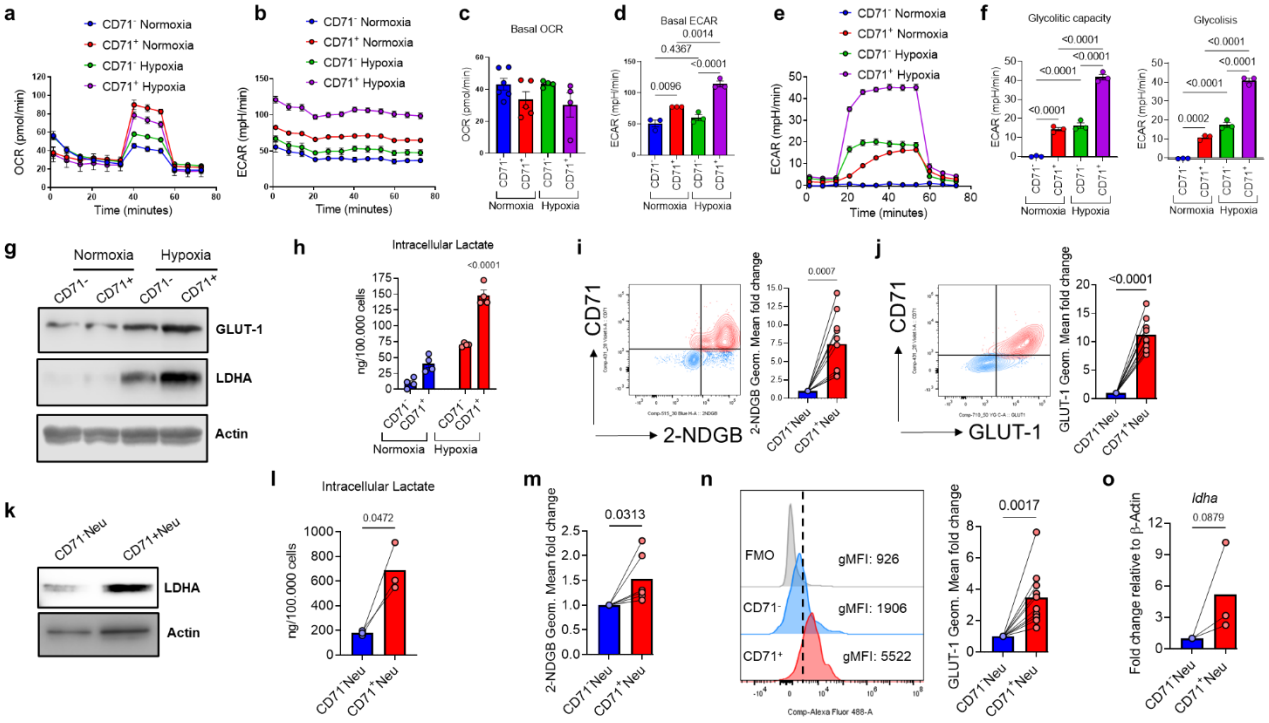

Fig. 5 - Hypoxia boosts glucose metabolism in CD71⁺Neu.

(**a**). Representative Mito Stress Test kinetic plot wherein values for Oxygen Consumption Rate (OCR, pmol/min) are plotted versus time. Note that oligomycin A was injected at 18 min followed by FCCP injection at 36 min and rotenone and antimycin A injection at 54 min. (**b**). Representative Mito Stress Test kinetic plot wherein values for extracellular acidification rate (ECAR, mpH/min) are plotted versus time. Note that oligomycin A was injected at 18 min followed by FCCP injection at 36 min and rotenone and antimycin A injection at 54 min. (**c**). Summaries of OCR data representative of the basal OCR levels. (**d**). Summaries of ECAR data representative of the basal ECAR levels. (**e**). Representative Glyco Stress Test kinetic plot wherein values for extracellular acidification rate (ECAR, mpH/min) are plotted versus time. Note that glucose was injected at 18 min followed by oligomycin A injection at 36 min and 2-DG injection at 54 min. (**f**). Summaries of ECAR data representative of the Glycolytic capacity (left) and glycolysis (right). (**g**). WB of indicated markers in *in vitro* Neu. (**h**). Intracellular lactate levels in *in vitro* Neu (Lactate assay kit). (**i**). 2-NDGB uptake in murine tumor (SB28) derived Neu measured by FACS. (**j**). GLUT-1 expression in murine tumor (SB28) derived Neu measured by FACS. (**k**). WB of indicated markers in tumor derived Neu. (**l**). Intracellular lactate levels in *in vitro* Neu (Lactate assay kit). (**m**). 2-NDGB uptake in human tumor derived Neu measured by FACS. (**n**). GLUT-1 expression in human tumor derived Neu measured by FACS. (**o**). *ldha* expression by RT-qPCR in human tumor derived Neu. All data are presented as mean ± SEM. Statistical analysis was performed using one-way ANOVA with Tukey's post hoc test (**c**, **d**, and **f**), two-way ANOVA with Tukey's post hoc test (**h**), and paired two-sided Student's *t*-tests (**i**, **j**, **l**, **m**, **n** and **o**).

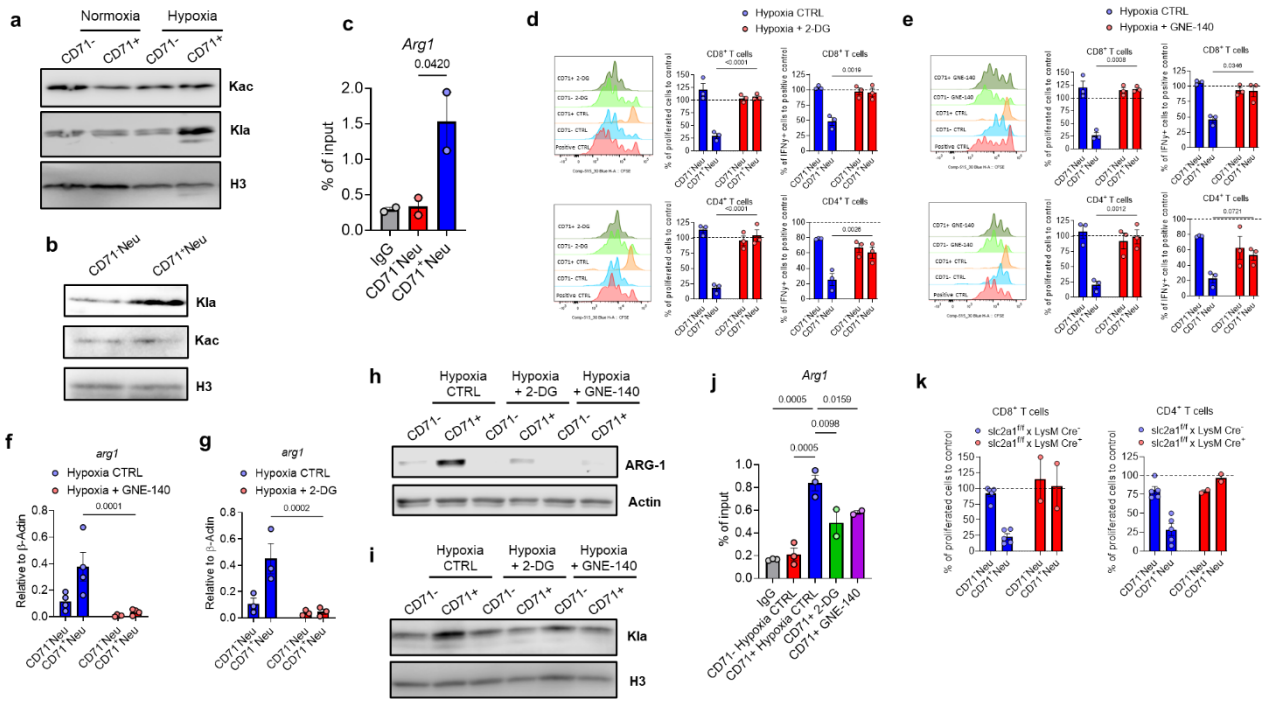

Fig. 6 - Glycolysis and lactate govern the immunosuppressive activity of CD71⁺Neu through histone lactylation.

(**a**). WB of indicated markers in *in vitro* Neu. (**b**). WB of indicated markers in tumor derived Neu. (**c**). CUT&RUN-RT-qPCR analysis for the association of Kla with the promoter of *Arg1* gene in tumor derived Neu. (**d**). Suppressive ability of *in vitro* hypoxic CD71⁺Neu and CD71⁻Neu treated with 2-DG on $CD8^+$ and $CD4^+$ T cells proliferation (left), measured as CFSE dilution, and IFN-γ production (right), by FACS. (**e**). Suppressive ability of *in vitro* hypoxic CD71⁺Neu and CD71⁻Neu treated with GNE-140 on $CD8^+$ and $CD4^+$ T cells proliferation (left), measured as CFSE dilution, and IFN-γ production (right), by FACS. (**f**). *arg1* expression by RT-qPCR in *in vitro* hypoxic CD71⁺Neu and CD71⁻Neu treated with 2-DG. (**g**). *arg1* expression by RT-qPCR in *in vitro* hypoxic CD71⁺Neu and CD71⁻Neu treated with GNE-140. (**h**). WB of indicated markers in *in vitro* hypoxic Neu treated with 2-DG and GNE-140. (**i**). WB of indicated markers in *in vitro* hypoxic Neu treated with 2-DG and GNE-140. (**j**). CUT&RUN-RT-qPCR analysis for the association of Kla with the promoter of *Arg1* gene in *in vitro* hypoxic Neu treated with 2-DG and GNE-140. (**k**). Suppressive ability of tumor (SB28) derived CD71⁺Neu and CD71⁻Neu from control ($Slc2a1^{f/f}$ $LysM^{CRE-}$) vs GLUT-1 CKO ($Slc2a1^{f/f}$ $LysM^{CRE+}$) mice on $CD8^+$ and $CD4^+$ T cells proliferation, measured as CFSE dilution by FACS. All data are presented as mean ± SEM. Statistical analysis was performed using two-way ANOVA with Holm-Šidák's post hoc test (**c** and **j**) and two-way ANOVA with Tukey's post hoc test (**d**, **e**, **f**, **g** and **k**).

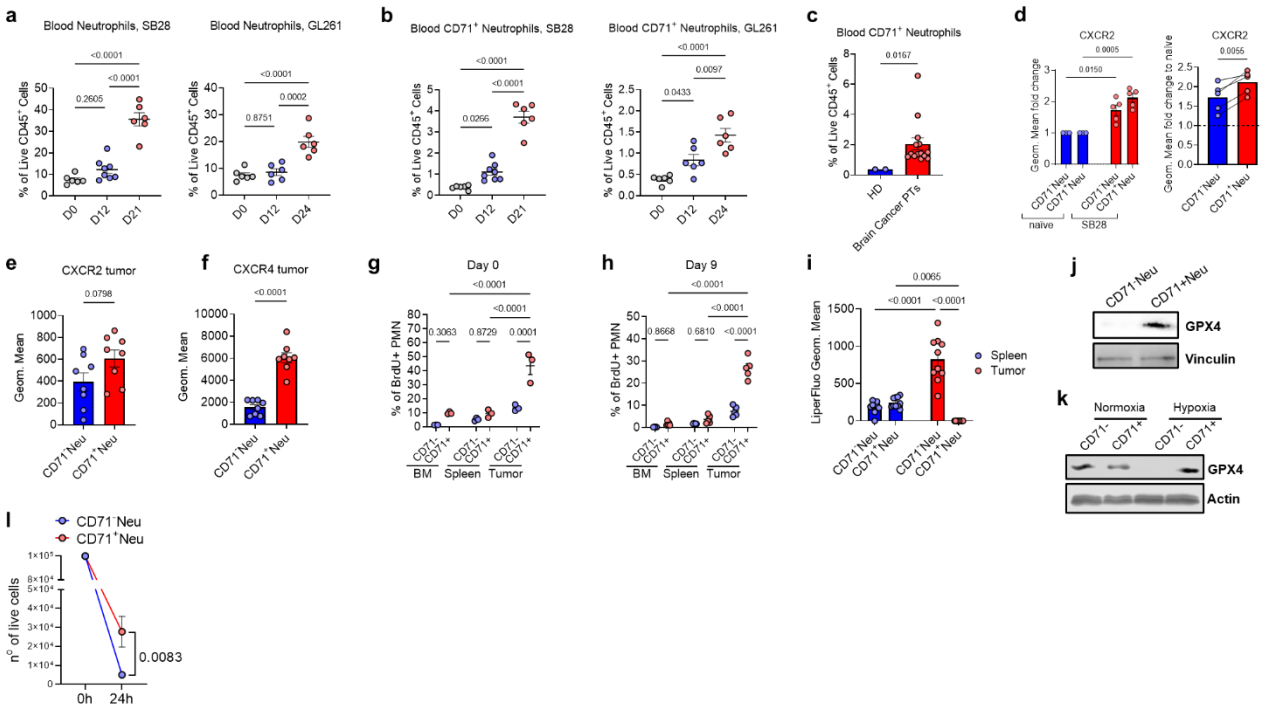

Fig. 7 - CD71⁺Neu are mobilized from BM during tumor progression and persist longer within the TME.

(**a**). Frequency of Neu out of live CD45⁺ cells in the blood of SB28 (left) and GL261 (right) GBM murine models over time by FACS. (**b**). Frequency of CD71⁺Neu out of live CD45⁺ cells in the blood of SB28 (left) and GL261 (right) GBM murine models over time by FACS. (**c**). Frequency of CD71⁺Neu out of live CD45⁺ cells in the blood of healthy donor (HD) vs brain cancer patients by FACS. (**d**). CXCR2 Geom. Mean fold change of SB28-bearing mice BM derived CD71⁺Neu vs CD71⁻Neu to their naïve counterpart, by FACS. (**e**). CXCR2 expression by tumor (SB28) derived Neu by FACS. (**f**). CXCR4 expression by tumor (SB28) derived Neu by FACS. (**g**). *In vivo* BrdU incorporation by Neu 3h post BrdU administration, measured by FACS. (**h**). *In vivo* BrdU persistence in Neu 9 days post BrdU administration, measured by FACS. (**i**). LiperFluo staining on tumor (SB28) derived Neu by FACS. (**j**). WB of indicated markers in tumor (SB28) derived Neu. (**k**). WB of indicated markers in *in vitro* Neu. (**l**). Survival of *in vitro* hypoxic Neu. All data are presented as mean ± SEM. Statistical analysis was performed using one-way ANOVA with Tukey's post hoc test (**a**, **b** and **d**), unpaired two-sided Student's *t*-tests (**c**, **e** and **f**), paired two-sided Student's *t*-tests (**d**), two-way ANOVA with Tukey's post hoc test (**g**, **h** and **i**) and two-way ANOVA with Holm-Šidák's post hoc test (**l**).

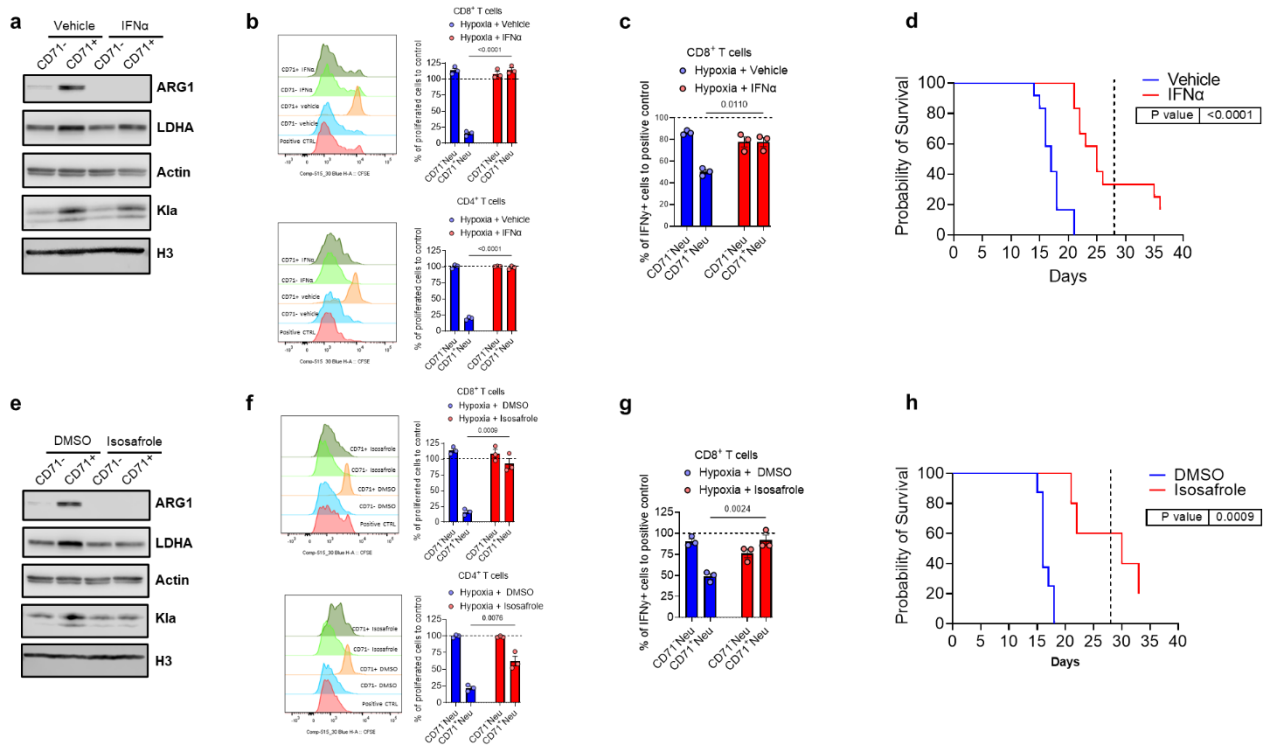

Fig. 8 - LDHA targeting through IFNα and Isosafrole prolonged the survival of GBM bearing mice.

(**a**). WB of indicated markers in *in vitro* hypoxic Neu after treatment with IFNα. (**b**). Suppressive ability of *in vitro* hypoxic CD71$^+$Neu and CD71$^-$Neu treated with IFNα on CD8$^+$ and CD4$^+$ T cells proliferation measured as CFSE dilution by FACS. (**c**). Suppressive ability of *in vitro* hypoxic CD71$^+$Neu and CD71$^-$Neu treated with IFNα on CD8$^+$ T cells IFN-γ production by FACS. (**d**). Kaplan-Meier representation of SB28-bearing mice treated with vehicle or IFNα. The dashed line indicates the ending of treatment. (**e**). WB of indicated markers in *in vitro* hypoxic Neu after treatment with Isosafrole. (**f**). Suppressive ability of *in vitro* hypoxic CD71$^+$Neu and CD71$^-$Neu treated with Isosafrole on CD8$^+$ and CD4$^+$ T cells proliferation measured as CFSE dilution by FACS. (**g**). Suppressive ability of *in vitro* hypoxic CD71$^+$Neu and CD71$^-$Neu treated with Isosafrole on CD8$^+$ T cells IFN-γ production by FACS. (**h**). Kaplan-Meier representation of SB28-bearing mice treated with DMSO or Isosafrole. The dashed line indicates the ending of treatment. All data are presented as mean ± SEM. Statistical analysis was performed using two-way ANOVA with Tukey's post hoc test (**b**, **c**, **f** and **g**) and Kaplan-Meier method and log-rank test (**d** and **h**).

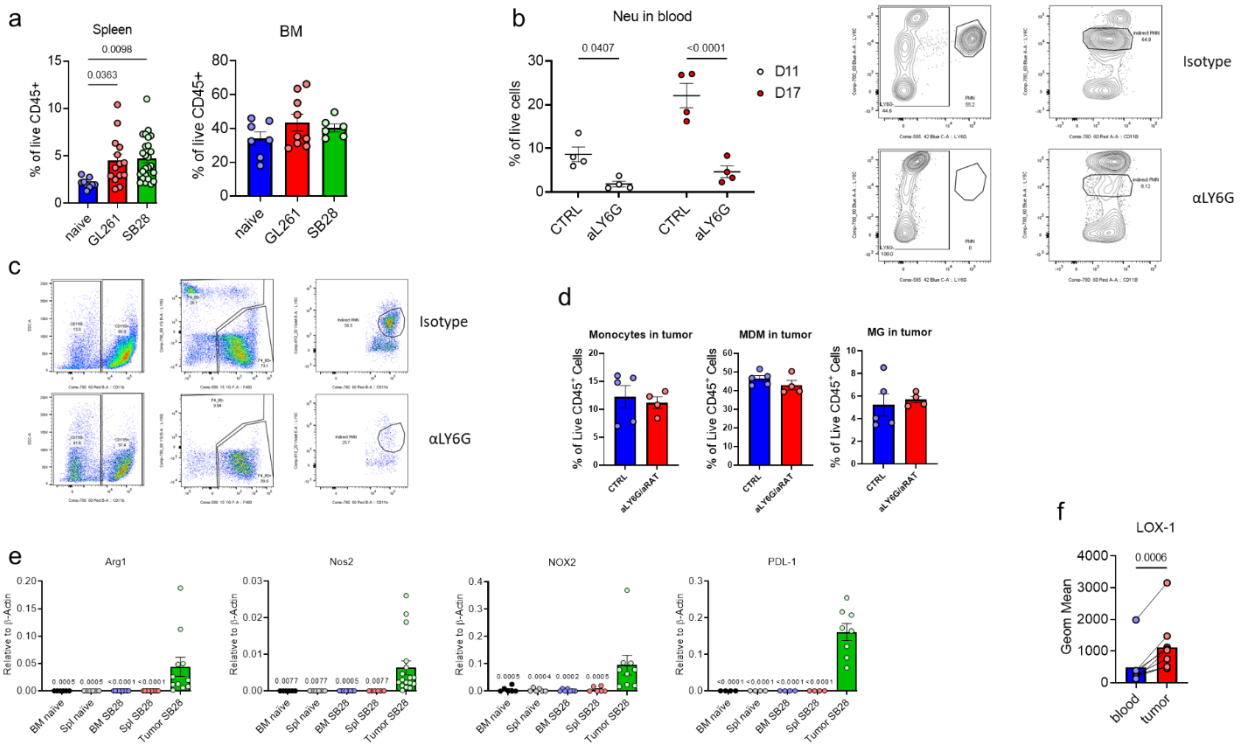

Supplementary Fig. 1 - Neutrophils infiltrate brain tumors acquiring immunosuppressive features.

(**a**). Frequency of Neu out of live CD45⁺ cells in the spleen and BM of naïve vs GBM-bearing mice by FACS. (**b**). Frequency of Neu out of live CD45⁺ cells in the blood of SB28-bearing mice (left) and direct vs indirect Neu gating strategy (right) after Neu depletion by FACS. (**c**). Indirect Neu gating strategy in tumor after Neu depletion by FACS. (**d**). Frequency of monocytes, MDM and MG out of live CD45⁺ cells in tumor of SB28-bearing mice after Neu depletion by FACS. (**e**). RT-qPCR of the indicated markers of *in vivo* Neu from naïve vs tumor (SB28)-bearing mice. (**f**). LOX-1 expression by human patients' blood vs tumor derived Neu by FACS. All data are presented as mean ± SEM. Statistical analysis was performed using one-way ANOVA with Tukey's post hoc test (**a**), two-way ANOVA with Tukey's post hoc test (**b** and **e**), unpaired two-sided Student's *t*-tests (**d**) and paired two-sided Student's *t*-tests (**f**).

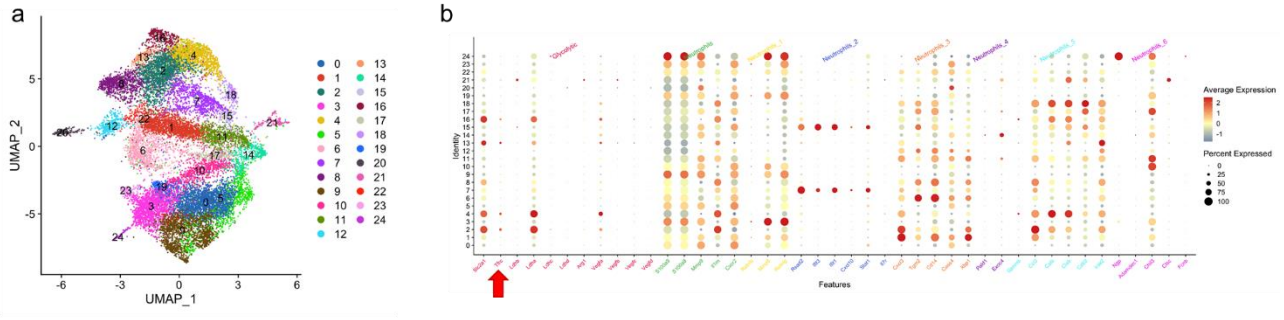

c

ClusterName	Blood Neu_1	Blood Neu_2	Tumor Neu_1	Tumor Neu_2
celltype_1	2620	3846	366	572
celltype_2	24	20	7	8
celltype_3	4	3	1015	1902
celltype_4	31	42	831	1549
celltype_5	36	99	562	516
celltype_6	113	229	229	400
celltype_7	5	7	107	189
celltype_8	2	3	333	438
celltype_9	0	0	115	119

Supplementary Fig. 2 - A population of glycolytic neutrophils expressing the CD71 receptor is expanded in brain tumors where it acquires a hypoxic signature.

(**a**). Unsupervised clustering of Neu. (**b**). Most expressed genes in the different clusters of Neu. The arrow indicates the *tfrc* gene. (**c**). Cell type numbers in the different samples.

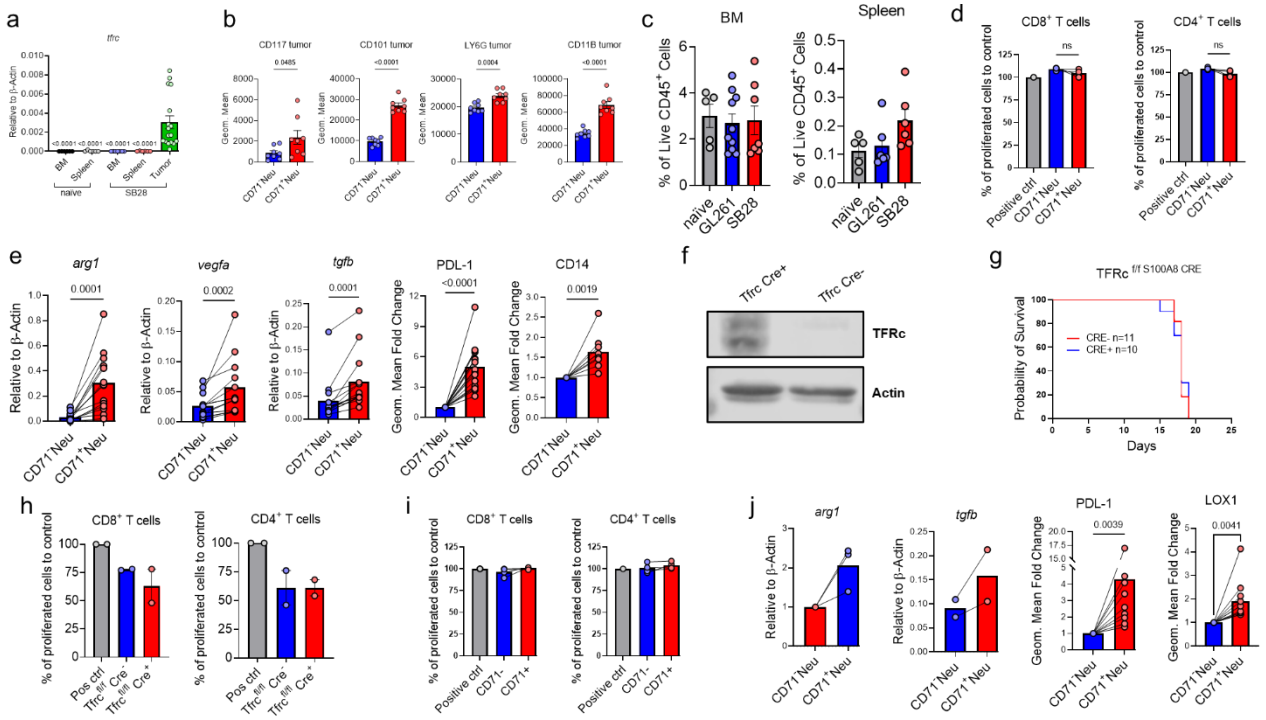

Supplementary Fig. 3 - CD71⁺Neu are critical contributors to the immunosuppressive activity associated with neutrophils in brain tumors.

(**a**). *tfrc* expression by RT-qPCR of *in vivo* Neu from naïve vs tumor (SB28)-bearing mice. (**b**). Geom. Mean of the indicated markers of tumor (SB28) derived Neu by FACS. (**c**). Frequency of CD71⁺Neu out of live CD45⁺ cells in the spleen and BM of naïve vs GBM-bearing mice by FACS. (**d**). Suppressive ability of BM derived CD71⁺Neu and CD71⁻Neu FACS sorted from SB28-bearing mice on CD8⁺ and CD4⁺ T cells proliferation, measured as CFSE dilution by FACS. (**e**). RT-qPCR or Geom. Mean fold change by FACS of the indicated markers of *in vivo* Neu from SB28-bearing mice. (**f**). WB of indicated markers in tumor (SB28) derived Neu. (**g**). Kaplan-Meier representation of SB28-bearing control (Tfrc$^{f/f}$ S100A8^{CRE-}) vs CD71 CKO (Tfrc$^{f/f}$ S100A8^{CRE+}) mice. (**h**). Suppressive ability of tumor (SB28) derived Neu from control (Tfrc$^{f/f}$ S100A8^{CRE-}) vs CD71 CKO (Tfrc$^{f/f}$ S100A8^{CRE+}) mice on CD8⁺ and CD4⁺ T cells proliferation, measured as CFSE dilution by FACS. (**i**). Suppressive ability of blood derived CD71⁺Neu and CD71⁻Neu FACS sorted from brain cancer patients on CD8⁺ and CD4⁺ T cells proliferation, measured as CFSE dilution by FACS. (**j**). RT-qPCR or Geom. Mean fold change by FACS of the indicated markers of *in vivo* Neu from human brain tumors. All data are presented as mean ± SEM. Statistical analysis was performed using two-way ANOVA with Tukey's post hoc test (**a**), unpaired two-sided Student's *t*-tests (**b**), one-way ANOVA with Tukey's post hoc test (**c** and **h**), paired two-sided Student's *t*-tests (**d**, **e**, **i** and **j**) and Kaplan-Meier method and log-rank test (**g**).

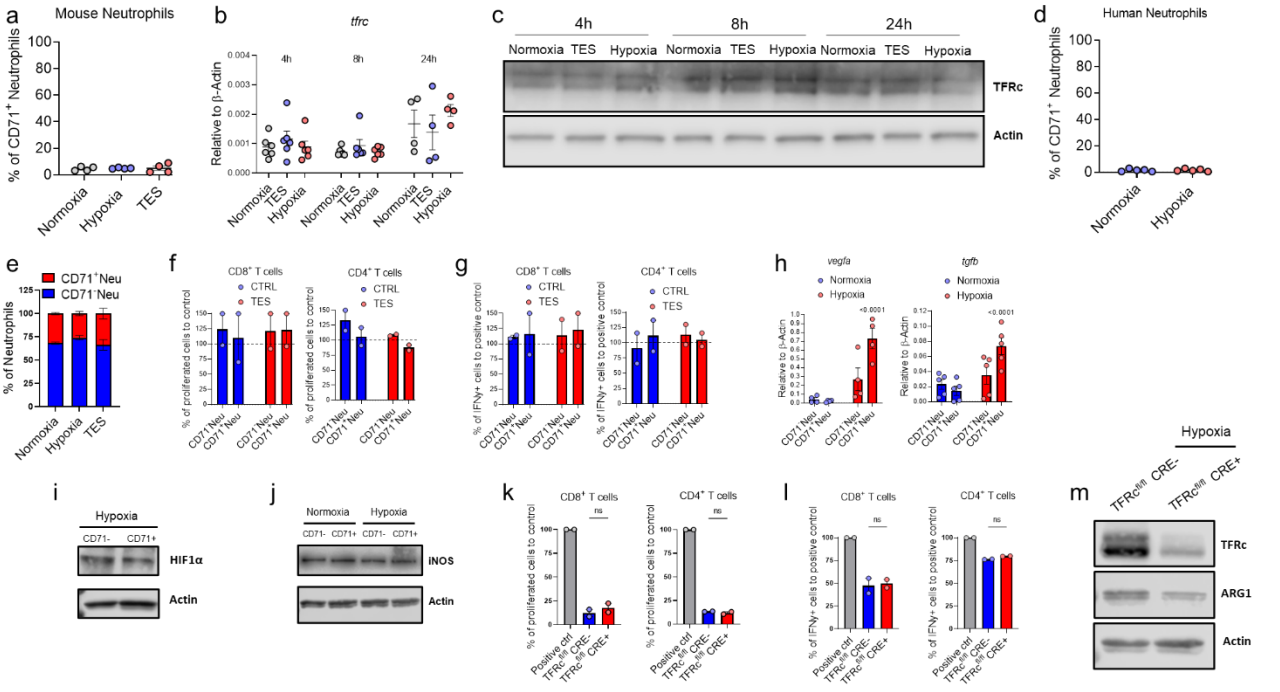

Supplementary Fig. 4 - Hypoxia drives immunosuppressive function and ARG-1 expression in CD71⁺Neu.

(**a**). Frequency of CD71⁺Neu in *in vitro* murine mature Neu. (**b**). *tfrc* expression by RT-qPCR of *in vitro* murine mature Neu. (**c**). WB of indicated markers in *in vitro* murine mature Neu. (**d**). Frequency of CD71⁺Neu in *in vitro* human mature Neu. (**e**). Frequency of CD71⁺Neu in *in vitro* BM precursors derived Neu. (**f**). Suppressive ability of *in vitro* CD71⁺Neu and CD71⁻Neu on CD8⁺ and CD4⁺ T cells proliferation, measured as CFSE dilution by FACS. (**g**). Suppressive ability of *in vitro* CD71⁺Neu and CD71⁻Neu on CD8⁺ and CD4⁺ T cells IFN-γ production by FACS. (**h**). RT-QPCR of the indicated markers of *in vitro* Neu. (**i**). WB of indicated markers in *in vitro* hypoxic Neu. (**j**). WB of indicated markers in *in vitro* Neu. (**k**). Suppressive ability of *in vitro* generated Neu from the BM of control ($Tfrc^{f/f}$ $S100A8^{CRE-}$) vs CD71 CKO ($Tfrc^{f/f}$ $S100A8^{CRE+}$) mice on CD8⁺ and CD4⁺ T cells proliferation, measured as CFSE dilution by FACS. (**l**). Suppressive ability of *in vitro* generated Neu from the BM of control ($Tfrc^{f/f}$ $S100A8^{CRE-}$) vs CD71 CKO ($Tfrc^{f/f}$ $S100A8^{CRE+}$) mice on CD8⁺ and CD4⁺ T cells IFN-γ production, by FACS. (**m**). WB of indicated markers in *in vitro* hypoxic Neu generated from the BM of control ($Tfrc^{f/f}$ $S100A8^{CRE-}$) vs CD71 CKO ($Tfrc^{f/f}$ $S100A8^{CRE+}$) mice. All data are presented as mean ± SEM. Statistical analysis was performed using one-way ANOVA with Tukey's post hoc test (**a**, **e**, **k** and **l**), two-way ANOVA with Tukey's post hoc test (**b**, **f**, **g** and **h**) and unpaired two-sided Student's *t*-tests (**d**).

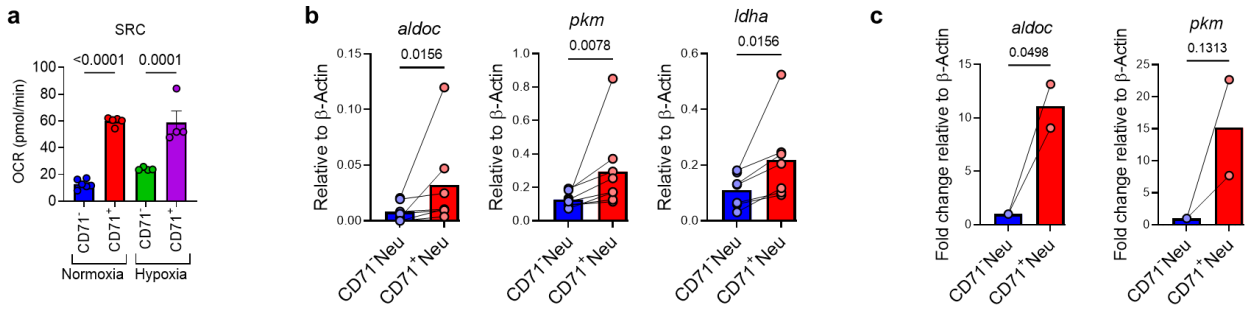

Supplementary Fig. 5 - Hypoxia boosts glucose metabolism in CD71⁺Neu.

(**a**). Summaries of OCR data representative of the Spare Respiratory Capacity. (**b**). RT-qPCR of the indicated markers of *in vivo* tumor (SB28) derived Neu. (**c**). RT-qPCR of the indicated markers of *in vivo* Neu from human brain tumors. All data are presented as mean ± SEM. Statistical analysis was performed using one-way ANOVA with Tukey's post hoc test (**a**) and paired two-sided Student's *t*-tests (**b** and **c**).

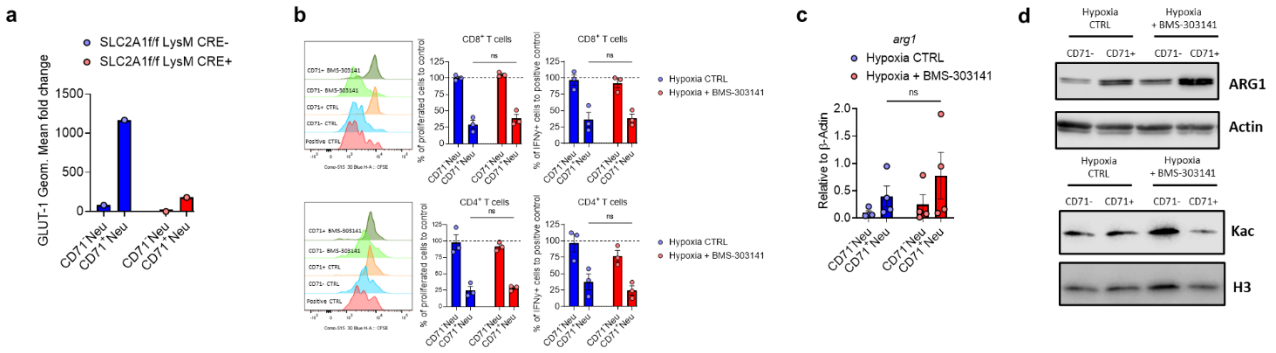

Supplementary Fig. 6 - Glycolysis and lactate govern the immunosuppressive activity of CD71^{+}Neu through histone lactylation.

(**a**). GLUT-1 expression by FACS of tumor (SB28) derived CD71^{+}Neu and CD71^{-}Neu from control (Slc2a1$^{f/f}$ LysM^{CRE-}) vs GLUT-1 CKO (Slc2a1$^{f/f}$ LysM^{CRE+}) mice (**b**). Suppressive ability of *in vitro* hypoxic CD71^{+}Neu and CD71^{-}Neu treated with BMS-303141 on CD8^{+} and CD4^{+} T cells proliferation (left), measured as CFSE dilution, and IFN-γ production (right), by FACS. (**c**). *arg1* expression by RT-qPCR in *in vitro* hypoxic CD71^{+}Neu and CD71^{-}Neu treated with BMS-303141. (**h**). WB of indicated markers in *in vitro* hypoxic Neu treated with BMS-303141. All data are presented as mean ± SEM. Statistical analysis was performed using two-way ANOVA with Tukey's post hoc test.

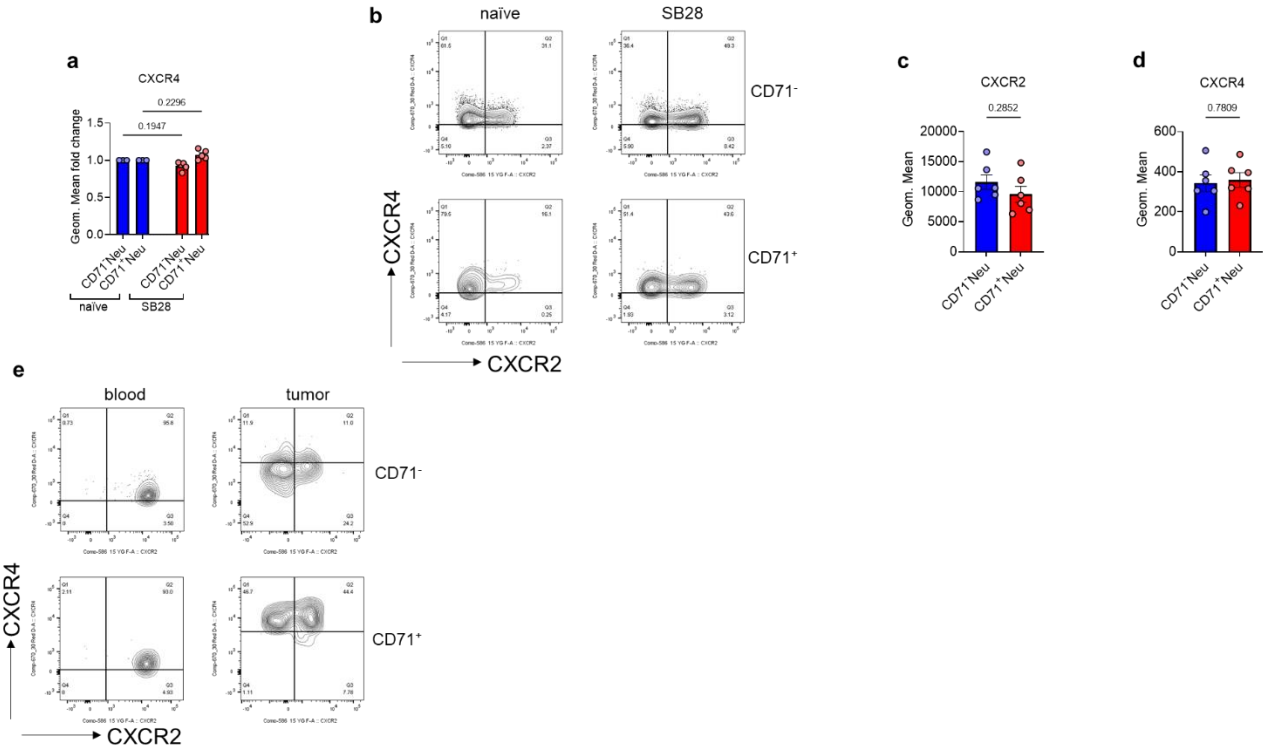

Supplementary Fig. 7 - CD71⁺Neu are mobilized from BM during tumor progression and persist longer within the TME.

(**a**). CXCR4 Geom. Mean fold change of SB28-bearing mice BM derived CD71⁺Neu vs CD71⁻Neu to their naïve counterpart, by FACS. (**b**). CXCR4 and CXCR2 expression by FACS in naïve vs SB28-bearing mice BM derived Neu. (**c**). CXCR2 expression by blood derived Neu in SB28-bearing mice by FACS. (**d**). CXCR4 expression by blood derived Neu in SB28-bearing mice by FACS. (**e**). CXCR4 and CXCR2 expression by FACS in blood vs tumor derived Neu in SB28-bearing mice. All data are presented as mean ± SEM. Statistical analysis was performed using one-way ANOVA with Tukey's post hoc test (**a**) and unpaired two-sided Student's *t*-tests (**c** and **d**).

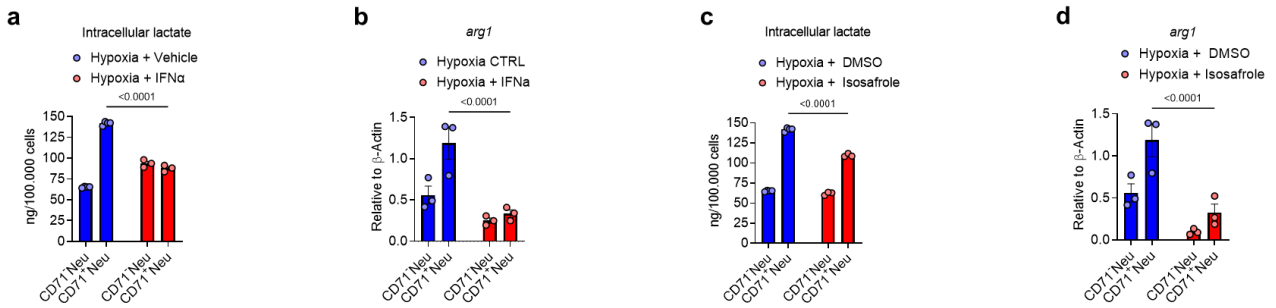

Fig. 8 - LDHA targeting through IFNα and Isosafrole prolonged the survival of GBM bearing mice.

(**a**). Intracellular lactate levels in *in vitro* hypoxic CD71^{+}Neu and CD71^{-}Neu treated with IFNα (Lactate assay kit). (**b**). *arg1* expression by RT-qPCR in *in vitro* hypoxic CD71^{+}Neu and CD71^{-}Neu treated with BMS-303141. (**c**). Intracellular lactate levels in *in vitro* hypoxic CD71^{+}Neu and CD71^{-}Neu treated with Isosafrole (Lactate assay kit). (**b**). *arg1* expression by RT-qPCR in *in vitro* hypoxic CD71^{+}Neu and CD71^{-}Neu treated with Isosafrole.

References

1 Cancer Genome Atlas Research, N. *et al.* Comprehensive, Integrative Genomic Analysis of Diffuse Lower-Grade Gliomas. *N Engl J Med* **372**, 2481-2498 (2015). https://doi.org:10.1056/NEJMoa1402121

2 Verhaak, R. G. *et al.* Integrated genomic analysis identifies clinically relevant subtypes of glioblastoma characterized by abnormalities in PDGFRA, IDH1, EGFR, and NF1. *Cancer Cell* **17**, 98-110 (2010). https://doi.org:10.1016/j.ccr.2009.12.020

3 Davis, M. E. Glioblastoma: Overview of Disease and Treatment. *Clin J Oncol Nurs* **20**, S2-8 (2016). https://doi.org:10.1188/16.CJON.S1.2-8

4 Stupp, R. *et al.* Effect of Tumor-Treating Fields Plus Maintenance Temozolomide vs Maintenance Temozolomide Alone on Survival in Patients With Glioblastoma: A Randomized Clinical Trial. *JAMA* **318**, 2306-2316 (2017). https://doi.org:10.1001/jama.2017.18718

5 Wei, S. C., Duffy, C. R. & Allison, J. P. Fundamental Mechanisms of Immune Checkpoint Blockade Therapy. *Cancer Discov* **8**, 1069-1086 (2018). https://doi.org:10.1158/2159-8290.CD-18-0367

6 Sampson, J. H., Gunn, M. D., Fecci, P. E. & Ashley, D. M. Brain immunology and immunotherapy in brain tumours. *Nat Rev Cancer* **20**, 12-25 (2020). https://doi.org:10.1038/s41568-019-0224-7

7 Tomaszewski, W., Sanchez-Perez, L., Gajewski, T. F. & Sampson, J. H. Brain Tumor Microenvironment and Host State: Implications for Immunotherapy. *Clin Cancer Res* **25**, 4202-4210 (2019). https://doi.org:10.1158/1078-0432.CCR-18-1627

8 Aldape, K. *et al.* Challenges to curing primary brain tumours. *Nat Rev Clin Oncol* **16**, 509-520 (2019). https://doi.org:10.1038/s41571-019-0177-5

9 De Leo, A., Ugolini, A. & Veglia, F. Myeloid Cells in Glioblastoma Microenvironment. *Cells* **10** (2020). https://doi.org:10.3390/cells10010018

10 Rahimi Koshkaki, H. *et al.* Immunohistochemical Characterization of Immune Infiltrate in Tumor Microenvironment of Glioblastoma. *J Pers Med* **10** (2020). https://doi.org:10.3390/jpm10030112

11 Ransohoff, R. M. & Engelhardt, B. The anatomical and cellular basis of immune surveillance in the central nervous system. *Nat Rev Immunol* **12**, 623-635 (2012). https://doi.org:10.1038/nri3265

12 das Neves, S. P., Delivanoglou, N. & Da Mesquita, S. CNS-Draining Meningeal Lymphatic Vasculature: Roles, Conundrums and Future Challenges. *Front Pharmacol* **12**, 655052 (2021). https://doi.org:10.3389/fphar.2021.655052

13 Martinez-Lage, M. *et al.* Immune landscapes associated with different glioblastoma molecular subtypes. *Acta Neuropathol Commun* **7**, 203 (2019). https://doi.org:10.1186/s40478-019-0803-6

14 Amankulor, N. M. *et al.* Mutant IDH1 regulates the tumor-associated immune system in gliomas. *Genes Dev* **31**, 774-786 (2017). https://doi.org:10.1101/gad.294991.116

15 Jaillon, S. *et al.* Neutrophil diversity and plasticity in tumour progression and therapy. *Nat Rev Cancer* **20**, 485-503 (2020). https://doi.org:10.1038/s41568-020-0281-y

16 Veglia, F., Perego, M. & Gabrilovich, D. Myeloid-derived suppressor cells coming of age. *Nat Immunol* **19**, 108-119 (2018). https://doi.org:10.1038/s41590-017-0022-x

17 Shaul, M. E. & Fridlender, Z. G. Tumour-associated neutrophils in patients with cancer. *Nat Rev Clin Oncol* **16**, 601-620 (2019). https://doi.org:10.1038/s41571-019-0222-4

18 Gentles, A. J. *et al.* The prognostic landscape of genes and infiltrating immune cells across human cancers. *Nat Med* **21**, 938-945 (2015). https://doi.org:10.1038/nm.3909

19 Massara, M. *et al.* Neutrophils in Gliomas. *Front Immunol* **8**, 1349 (2017). https://doi.org:10.3389/fimmu.2017.01349

20 Zadora, P. *et al.* Preoperative neutrophil-lymphocyte count ratio helps predict the grade of glial tumor - a pilot study. *Neurol Neurochir Pol* **49**, 41-44 (2015). https://doi.org:10.1016/j.pjnns.2014.12.006

21 Bambury, R. M. *et al.* The association of pre-treatment neutrophil to lymphocyte ratio with overall survival in patients with glioblastoma multiforme. *J Neurooncol* **114**, 149-154 (2013). https://doi.org:10.1007/s11060-013-1164-9

22 Mason, M. *et al.* Neutrophil-lymphocyte ratio dynamics during concurrent chemo-radiotherapy for glioblastoma is an independent predictor for overall survival. *J Neurooncol* **132**, 463-471 (2017). https://doi.org:10.1007/s11060-017-2395-y

23 Fossati, G. *et al.* Neutrophil infiltration into human gliomas. *Acta Neuropathol* **98**, 349-354 (1999). https://doi.org:10.1007/s004010051093

24 Rahbar, A. *et al.* Enhanced neutrophil activity is associated with shorter time to tumor progression in glioblastoma patients. *Oncoimmunology* **5**, e1075693 (2016). https://doi.org:10.1080/2162402X.2015.1075693

25 Zhao, J. *et al.* Immune and genomic correlates of response to anti-PD-1 immunotherapy in glioblastoma. *Nat Med* **25**, 462-469 (2019). https://doi.org:10.1038/s41591-019-0349-y

26 Bayik, D. *et al.* Myeloid-Derived Suppressor Cell Subsets Drive Glioblastoma Growth in a Sex-Specific Manner. *Cancer Discov* **10**, 1210-1225 (2020). https://doi.org:10.1158/2159-8290.CD-19-1355

27 Wang, P. F. *et al.* Neutrophil depletion enhances the therapeutic effect of PD-1 antibody on glioma. *Aging (Albany NY)* **12**, 15290-15301 (2020). https://doi.org:10.18632/aging.103428

28 Hor, W. S., Huang, W. L., Lin, Y. S. & Yang, B. C. Cross-talk between tumor cells and neutrophils through the Fas (APO-1, CD95)/FasL system: human glioma cells enhance cell viability and stimulate cytokine production in neutrophils. *J Leukoc Biol* **73**, 363-368 (2003). https://doi.org:10.1189/jlb.0702375

29 Chio, C. C., Wang, Y. S., Chen, Y. L., Lin, S. J. & Yang, B. C. Down-regulation of Fas-L in glioma cells by ribozyme reduces cell apoptosis, tumour-infiltrating cells, and liver damage but accelerates tumour formation in nude mice. *Br J Cancer* **85**, 1185-1192 (2001). https://doi.org:10.1054/bjoc.2001.2055

30 Iwatsuki, K. *et al.* Elastase expression by infiltrating neutrophils in gliomas. *Neurol Res* **22**, 465-468 (2000). https://doi.org:10.1080/01616412.2000.11740701

31 Liang, J. *et al.* Neutrophils promote the malignant glioma phenotype through S100A4. *Clin Cancer Res* **20**, 187-198 (2014). https://doi.org:10.1158/1078-0432.CCR-13-1279

32 Manda-Handzlik, A. & Demkow, U. The Brain Entangled: The Contribution of Neutrophil Extracellular Traps to the Diseases of the Central Nervous System. *Cells* **8** (2019). https://doi.org:10.3390/cells8121477

33 Sippel, T. R. *et al.* Neutrophil degranulation and immunosuppression in patients with GBM: restoration of cellular immune function by targeting arginase I. *Clin Cancer Res* **17**, 6992-7002 (2011). https://doi.org:10.1158/1078-0432.CCR-11-1107

34 Condamine, T. *et al.* Lectin-type oxidized LDL receptor-1 distinguishes population of human polymorphonuclear myeloid-derived suppressor cells in cancer patients. *Sci Immunol* **1** (2016). https://doi.org:10.1126/sciimmunol.aaf8943

35 Yee, P. P. *et al.* Neutrophil-induced ferroptosis promotes tumor necrosis in glioblastoma progression. *Nat Commun* **11**, 5424 (2020). https://doi.org:10.1038/s41467-020-19193-y

36 Ng, L. G., Ostuni, R. & Hidalgo, A. Heterogeneity of neutrophils. *Nat Rev Immunol* **19**, 255-265 (2019). https://doi.org:10.1038/s41577-019-0141-8

37 Veglia, F. *et al.* Analysis of classical neutrophils and polymorphonuclear myeloid-derived suppressor cells in cancer patients and tumor-bearing mice. *J Exp Med* **218** (2021). https://doi.org:10.1084/jem.20201803

38 Sagiv, J. Y. *et al.* Phenotypic diversity and plasticity in circulating neutrophil subpopulations in cancer. *Cell Rep* **10**, 562-573 (2015). https://doi.org:10.1016/j.celrep.2014.12.039

39 Veglia, F., Sanseviero, E. & Gabrilovich, D. I. Myeloid-derived suppressor cells in the era of increasing myeloid cell diversity. *Nat Rev Immunol* **21**, 485-498 (2021). https://doi.org:10.1038/s41577-020-00490-y

40 Quail, D. F. *et al.* Neutrophil phenotypes and functions in cancer: A consensus statement. *J Exp Med* **219** (2022). https://doi.org:10.1084/jem.20220011

41 Hedrick, C. C. & Malanchi, I. Neutrophils in cancer: heterogeneous and multifaceted. *Nat Rev Immunol* **22**, 173-187 (2022). https://doi.org:10.1038/s41577-021-00571-6
42 Boivin, G. *et al.* Durable and controlled depletion of neutrophils in mice. *Nat Commun* **11**, 2762 (2020). https://doi.org:10.1038/s41467-020-16596-9
43 Genoud, V. *et al.* Responsiveness to anti-PD-1 and anti-CTLA-4 immune checkpoint blockade in SB28 and GL261 mouse glioma models. *Oncoimmunology* **7**, e1501137 (2018). https://doi.org:10.1080/2162402X.2018.1501137
44 Ohgaki, H. & Kleihues, P. Population-based studies on incidence, survival rates, and genetic alterations in astrocytic and oligodendroglial gliomas. *J Neuropathol Exp Neurol* **64**, 479-489 (2005). https://doi.org:10.1093/jnen/64.6.479
45 Lun, A. T., Bach, K. & Marioni, J. C. Pooling across cells to normalize single-cell RNA sequencing data with many zero counts. *Genome Biol* **17**, 75 (2016). https://doi.org:10.1186/s13059-016-0947-7
46 McCarthy, D. J., Campbell, K. R., Lun, A. T. & Wills, Q. F. Scater: pre-processing, quality control, normalization and visualization of single-cell RNA-seq data in R. *Bioinformatics* **33**, 1179-1186 (2017). https://doi.org:10.1093/bioinformatics/btw777
47 Stuart, T. *et al.* Comprehensive Integration of Single-Cell Data. *Cell* **177**, 1888-1902 e1821 (2019). https://doi.org:10.1016/j.cell.2019.05.031
48 Heng, T. S., Painter, M. W. & Immunological Genome Project, C. The Immunological Genome Project: networks of gene expression in immune cells. *Nat Immunol* **9**, 1091-1094 (2008). https://doi.org:10.1038/ni1008-1091
49 Benayoun, B. A. *et al.* Remodeling of epigenome and transcriptome landscapes with aging in mice reveals widespread induction of inflammatory responses. *Genome Res* **29**, 697-709 (2019). https://doi.org:10.1101/gr.240093.118
50 Aran, D. *et al.* Reference-based analysis of lung single-cell sequencing reveals a transitional profibrotic macrophage. *Nat Immunol* **20**, 163-172 (2019). https://doi.org:10.1038/s41590-018-0276-y
51 Becht, E. *et al.* Dimensionality reduction for visualizing single-cell data using UMAP. *Nat Biotechnol* (2018). https://doi.org:10.1038/nbt.4314
52 Veglia, F. *et al.* Fatty acid transport protein 2 reprograms neutrophils in cancer. *Nature* **569**, 73-78 (2019). https://doi.org:10.1038/s41586-019-1118-2
53 Bhandari, V. *et al.* Molecular landmarks of tumor hypoxia across cancer types. *Nat Genet* **51**, 308-318 (2019). https://doi.org:10.1038/s41588-018-0318-2
54 Park, J. H. & Lee, H. K. Current Understanding of Hypoxia in Glioblastoma Multiforme and Its Response to Immunotherapy. *Cancers (Basel)* **14** (2022). https://doi.org:10.3390/cancers14051176
55 Dinh, H. Q. *et al.* Coexpression of CD71 and CD117 Identifies an Early Unipotent Neutrophil Progenitor Population in Human Bone Marrow. *Immunity* **53**, 319-334 e316 (2020). https://doi.org:10.1016/j.immuni.2020.07.017
56 Ugolini, A. & Nuti, M. CD137(+) T-Cells: Protagonists of the Immunotherapy Revolution. *Cancers (Basel)* **13** (2021). https://doi.org:10.3390/cancers13030456
57 Ugolini, A. *et al.* IgM-Rheumatoid factor confers primary resistance to anti-PD-1 immunotherapies in NSCLC patients by reducing CD137(+)T-cells. *EBioMedicine* **62**, 103098 (2020). https://doi.org:10.1016/j.ebiom.2020.103098
58 Zizzari, I. G. *et al.* Circulating CD137+ T Cells Correlate with Improved Response to Anti-PD1 Immunotherapy in Patients with Cancer. *Clin Cancer Res* **28**, 1027-1037 (2022). https://doi.org:10.1158/1078-0432.CCR-21-2918
59 Tacchini, L., Bianchi, L., Bernelli-Zazzera, A. & Cairo, G. Transferrin receptor induction by hypoxia. HIF-1-mediated transcriptional activation and cell-specific post-transcriptional regulation. *J Biol Chem* **274**, 24142-24146 (1999). https://doi.org:10.1074/jbc.274.34.24142
60 Fagundes, R. R. *et al.* HIF1alpha-Dependent Induction of TFRC by a Combination of Intestinal Inflammation and Systemic Iron Deficiency in Inflammatory Bowel Disease. *Front Physiol* **13**, 889091 (2022). https://doi.org:10.3389/fphys.2022.889091

61 Abou Khouzam, R. *et al.* The Effect of Hypoxia and Hypoxia-Associated Pathways in the Regulation of Antitumor Response: Friends or Foes? *Front Immunol* **13**, 828875 (2022). https://doi.org:10.3389/fimmu.2022.828875
62 Zhang, D. *et al.* Metabolic regulation of gene expression by histone lactylation. *Nature* **574**, 575-580 (2019). https://doi.org:10.1038/s41586-019-1678-1
63 Wang, N. *et al.* Histone Lactylation Boosts Reparative Gene Activation Post-Myocardial Infarction. *Circ Res* **131**, 893-908 (2022). https://doi.org:10.1161/CIRCRESAHA.122.320488
64 Noe, J. T. *et al.* Lactate supports a metabolic-epigenetic link in macrophage polarization. *Sci Adv* **7**, eabi8602 (2021). https://doi.org:10.1126/sciadv.abi8602
65 Yang, Q. *et al.* Cross talk between histone deacetylase 4 and STAT6 in the transcriptional regulation of arginase 1 during mouse dendritic cell differentiation. *Mol Cell Biol* **35**, 63-75 (2015). https://doi.org:10.1128/MCB.00805-14
66 Covarrubias, A. J. *et al.* Akt-mTORC1 signaling regulates Acly to integrate metabolic input to control of macrophage activation. *Elife* **5** (2016). https://doi.org:10.7554/eLife.11612
67 Huang, M. *et al.* Microglial immune regulation by epigenetic reprogramming through histone H3K27 acetylation in neuroinflammation. *Front Immunol* **14**, 1052925 (2023). https://doi.org:10.3389/fimmu.2023.1052925
68 denDekker, A. D. *et al.* TNF-alpha regulates diabetic macrophage function through the histone acetyltransferase MOF. *JCI Insight* **5** (2020). https://doi.org:10.1172/jci.insight.132306
69 Mullican, S. E. *et al.* Histone deacetylase 3 is an epigenomic brake in macrophage alternative activation. *Genes Dev* **25**, 2480-2488 (2011). https://doi.org:10.1101/gad.175950.111
70 Lin, L. J. & Schultz, M. C. Promoter regulation by distinct mechanisms of functional interplay between lysine acetylase Rtt109 and histone chaperone Asf1. *Proc Natl Acad Sci U S A* **108**, 19599-19604 (2011). https://doi.org:10.1073/pnas.1111501108
71 de Almeida Nagata, D. E. *et al.* Regulation of Tumor-Associated Myeloid Cell Activity by CBP/EP300 Bromodomain Modulation of H3K27 Acetylation. *Cell Rep* **27**, 269-281 e264 (2019). https://doi.org:10.1016/j.celrep.2019.03.008
72 Guo, Q. *et al.* Inhibition of ACLY Leads to Suppression of Osteoclast Differentiation and Function Via Regulation of Histone Acetylation. *J Bone Miner Res* **36**, 2065-2080 (2021). https://doi.org:10.1002/jbmr.4399
73 Coffelt, S. B., Wellenstein, M. D. & de Visser, K. E. Neutrophils in cancer: neutral no more. *Nat Rev Cancer* **16**, 431-446 (2016). https://doi.org:10.1038/nrc.2016.52
74 Gabrilovich, D. I., Ostrand-Rosenberg, S. & Bronte, V. Coordinated regulation of myeloid cells by tumours. *Nat Rev Immunol* **12**, 253-268 (2012). https://doi.org:10.1038/nri3175
75 Peng, Z. *et al.* Tumors exploit CXCR4(hi)CD62L(lo) aged neutrophils to facilitate metastatic spread. *Oncoimmunology* **10**, 1870811 (2021). https://doi.org:10.1080/2162402X.2020.1870811
76 Tulotta, C. *et al.* CXCR4 signaling regulates metastatic onset by controlling neutrophil motility and response to malignant cells. *Sci Rep* **9**, 2399 (2019). https://doi.org:10.1038/s41598-019-38643-2
77 Ancey, P. B. *et al.* GLUT1 Expression in Tumor-Associated Neutrophils Promotes Lung Cancer Growth and Resistance to Radiotherapy. *Cancer Res* **81**, 2345-2357 (2021). https://doi.org:10.1158/0008-5472.CAN-20-2870
78 Erben, R. G., Odorfer, K. I., Siebenhutter, M., Weber, K. & Rohleder, S. Histological assessment of cellular half-life in tissues in vivo. *Histochem Cell Biol* **130**, 1041-1046 (2008). https://doi.org:10.1007/s00418-008-0470-3
79 Huang, Y. *et al.* TFRC promotes epithelial ovarian cancer cell proliferation and metastasis via up-regulation of AXIN2 expression. *Am J Cancer Res* **10**, 131-147 (2020).
80 Feng, H. *et al.* Transferrin Receptor Is a Specific Ferroptosis Marker. *Cell Rep* **30**, 3411-3423 e3417 (2020). https://doi.org:10.1016/j.celrep.2020.02.049
81 Wang, W. *et al.* CD8(+) T cells regulate tumour ferroptosis during cancer immunotherapy. *Nature* **569**, 270-274 (2019). https://doi.org:10.1038/s41586-019-1170-y

82 Seibt, T. M., Proneth, B. & Conrad, M. Role of GPX4 in ferroptosis and its pharmacological implication. *Free Radic Biol Med* **133**, 144-152 (2019). https://doi.org:10.1016/j.freeradbiomed.2018.09.014

83 Hu, B. *et al.* IFNalpha Potentiates Anti-PD-1 Efficacy by Remodeling Glucose Metabolism in the Hepatocellular Carcinoma Microenvironment. *Cancer Discov* **12**, 1718-1741 (2022). https://doi.org:10.1158/2159-8290.CD-21-1022

84 Sada, N., Lee, S., Katsu, T., Otsuki, T. & Inoue, T. Epilepsy treatment. Targeting LDH enzymes with a stiripentol analog to treat epilepsy. *Science* **347**, 1362-1367 (2015). https://doi.org:10.1126/science.aaa1299

85 Guyon, J. *et al.* Lactate dehydrogenases promote glioblastoma growth and invasion via a metabolic symbiosis. *EMBO Mol Med* **14**, e15343 (2022). https://doi.org:10.15252/emmm.202115343

86 Klemm, F. *et al.* Interrogation of the Microenvironmental Landscape in Brain Tumors Reveals Disease-Specific Alterations of Immune Cells. *Cell* **181**, 1643-1660 e1617 (2020). https://doi.org:10.1016/j.cell.2020.05.007

87 Friebel, E. *et al.* Single-Cell Mapping of Human Brain Cancer Reveals Tumor-Specific Instruction of Tissue-Invading Leukocytes. *Cell* **181**, 1626-1642 e1620 (2020). https://doi.org:10.1016/j.cell.2020.04.055

88 Yeo, A. T. *et al.* Single-cell RNA sequencing reveals evolution of immune landscape during glioblastoma progression. *Nat Immunol* **23**, 971-984 (2022). https://doi.org:10.1038/s41590-022-01215-0

89 Mishalian, I. *et al.* Tumor-associated neutrophils (TAN) develop pro-tumorigenic properties during tumor progression. *Cancer Immunol Immunother* **62**, 1745-1756 (2013). https://doi.org:10.1007/s00262-013-1476-9

90 Montaldo, E. *et al.* Cellular and transcriptional dynamics of human neutrophils at steady state and upon stress. *Nat Immunol* **23**, 1470-1483 (2022). https://doi.org:10.1038/s41590-022-01311-1

91 Gabrilovich, D. I. & Nagaraj, S. Myeloid-derived suppressor cells as regulators of the immune system. *Nat Rev Immunol* **9**, 162-174 (2009). https://doi.org:10.1038/nri2506

92 Wang, L. *et al.* Single-cell RNA-seq analysis reveals BHLHE40-driven pro-tumour neutrophils with hyperactivated glycolysis in pancreatic tumour microenvironment. *Gut* **72**, 958-971 (2023). https://doi.org:10.1136/gutjnl-2021-326070

93 Beppu, T. *et al.* Change of oxygen pressure in glioblastoma tissue under various conditions. *J Neurooncol* **58**, 47-52 (2002). https://doi.org:10.1023/a:1015832726054

94 Corzo, C. A. *et al.* HIF-1alpha regulates function and differentiation of myeloid-derived suppressor cells in the tumor microenvironment. *J Exp Med* **207**, 2439-2453 (2010). https://doi.org:10.1084/jem.20100587

95 Jamieson, T. *et al.* Inhibition of CXCR2 profoundly suppresses inflammation-driven and spontaneous tumorigenesis. *J Clin Invest* **122**, 3127-3144 (2012). https://doi.org:10.1172/JCI61067

96 Kim, R. *et al.* Ferroptosis of tumour neutrophils causes immune suppression in cancer. *Nature* **612**, 338-346 (2022). https://doi.org:10.1038/s41586-022-05443-0

97 Feng, Y. *et al.* Lactate dehydrogenase A: A key player in carcinogenesis and potential target in cancer therapy. *Cancer Med* **7**, 6124-6136 (2018). https://doi.org:10.1002/cam4.1820

98 Miyajima, H., Takahashi, Y., Suzuki, M., Shimizu, T. & Kaneko, E. Molecular characterization of gene expression in human lactate dehydrogenase-A deficiency. *Neurology* **43**, 1414-1419 (1993). https://doi.org:10.1212/wnl.43.7.1414

99 Kanno, T. *et al.* Lactate dehydrogenase M-subunit deficiency: a new type of hereditary exertional myopathy. *Clin Chim Acta* **173**, 89-98 (1988). https://doi.org:10.1016/0009-8981(88)90359-2

100 Guo, C. *et al.* Adjuvant Temozolomide Chemotherapy With or Without Interferon Alfa Among Patients With Newly Diagnosed High-grade Gliomas: A Randomized Clinical Trial. *JAMA Netw Open* **6**, e2253285 (2023). https://doi.org:10.1001/jamanetworkopen.2022.53285

Acknowledgments

To my family. To Rome. To Tampa.

Main studies carried out during the PhD

1) Probing neutrophils heterogeneity in Glioblastoma: how the metabolism shapes the function of immunosuppressive CD71+Neutrophils.
2) Elucidating the role of glycolysis in reprogramming macrophages function in Glioblastoma.
3) The role of $CD137^+$ T cells in Glioblastoma.

Scientific production during the PhD

Manuscripts

1) Ilaria Grazia Zizzari, Alessandra Di Filippo, Fabio Scirocchi, Francesca Romana Di Pietro, Hassan Rahimi, **Alessio Ugolini**, Simone Scagnoli, Pamela Vernocchi, Federica Del Chierico, Lorenza Putignani, Aurelia Rughetti, Paolo Marchetti, Marianna Nuti, Andrea Botticelli* and Chiara Napoletano*. **Soluble Immune Checkpoints, Gut Metabolites and Performance Status as Parameters of Response to Nivolumab Treatment in NSCLC Patients.** *Journal of Personalized Medicine*, 2020/11/04. J. Pers. Med. 2020, 10(4), 208; https://doi.org/10.3390/jpm10040208.

2) **Alessio Ugolini**, Ilaria Grazia Zizzari, Fulvia Ceccarelli, Andrea Botticelli, Tania Colasanti, Lidia Strigari, Aurelia Rughetti, Hassan Rahimi, Fabrizio Conti, Guido Valesini, Paolo Marchetti, Marianna Nuti. **IgM-Rheumatoid factor confers primary resistance to anti-PD-1 Immunotherapies in NSCLC patients by reducing $CD137^+$ T cells.** *EBioMedicine,* 2020/11/06. https://doi.org/10.1016/j.ebiom.2020.103098.

3) Alessandra De Leo*, **Alessio Ugolini***, Filippo Veglia. **Myeloid Cells in Glioblastoma Microenvironment.** *Cells*, 2020 Dec 24;10(1):E18. doi: 10.3390/cells10010018.

4) **Alessio Ugolini,** Marianna Nuti. **CD137+ T cells: Protagonists of the Immunotherapy Revolution**. *Cancers* 2021, 13(3), 456; https://doi.org/10.3390/cancers13030456.

5) **Alessio Ugolini**, Marianna Nuti. **Rheumatoid Factor: A Novel Determiner in Cancer History**. *Cancers* 2021, 13(4), 591; https://doi.org/10.3390/cancers13040591.

6) Ilaria Grazia Zizzari, Alessandra Di Filippo, Andrea Botticelli, Lidia Strigari, Angelina Pernazza, Emma Rullo, Maria Gemma Pignataro, **Alessio Ugolini**, Fabio Scirocchi, Francesca Romana Di Pietro, Ernesto Rossi, Alain Gelibter, Giovanni Schinzari, Giulia D'Amati, Aurelia Rughetti, Paolo Marchetti, Marianna Nuti, and Chiara Napoletano. **Circulating CD137+ T Cells Correlate with Improved Response to Anti-PD1 Immunotherapy in Patients with Cancer.** *Clinical Cancer Research*, 2022 Mar 1;28(5):1027-1037. doi: 10.1158/1078-0432.CCR-21-2918.

7) Alessandra De Leo*, **Alessio Ugolini***, Xiaoqing Yu, Fabio Scirocchi, Barbara Peixoto, Delia Scocozza, Angelica Pace, Luca D'Angelo, James K. C. Liu, Arnold B. Etame, Aurelia Rughetti, Marianna Nuti, Michael A. Vogelbaum, Jose Conejo-Garcia, Paulo Rodriguez, Filippo Veglia. **Histone lactylation drives macrophage-suppressive activity in brain cancer**. *Immunity.* Revisions submitted, currently awaiting for editorial decision.

8) **Alessio Ugolini**, Alessandra De Leo, Xiaoqing Yu, Fabio Scirocchi, Barbara Peixoto, Delia Scocozza, Angelica Pace, Luca D'Angelo, James K. C. Liu, Arnold B. Etame, Aurelia Rughetti, Marianna Nuti, Michael A. Vogelbaum, Jose Conejo-Garcia, Paulo Rodriguez, Filippo Veglia. **Hypoxia-driven histone lactylation controls the function of immunosuppressive CD71+ neutrophils in Glioblastoma**. In preparation for submission.

Abstracts

1) **Alessio Ugolini**, Ilaria Grazia Zizzari, Fulvia Ceccarelli, Andrea Botticelli, Tania Colasanti, Lidia Strigari, Aurelia Rughetti, Hassan Rahimi, Fabrizio Conti, Guido Valesini, Paolo Marchetti, Marianna Nuti. **IgM-Rheumatoid Factor as a novel biomarker for a reduced survival in anti-PD-1 treated NSCLC patients through the decrease of CD137+ T cells.** *ESMO Immuno-Oncology Congress 2020*, Geneva, Switzerland, 9-12 December 2020. Published in *Annals of Oncology*, VOLUME 31, SUPPLEMENT 7, S1418, DECEMBER 01, 2020. DOI: https://doi.org/10.1016/j.annonc.2020.10.489. **Poster**.

2) Marco Filetti, Mario Occhipinti, Alessio Cirillo, Fabio Scirocchi, **Alessio Ugolini**, Manuela Petti, Raffaele Giusti, Pasquale Lombardi, Andrea Botticelli, Giuseppe Lo Russo, Filippo Maria De Braud, Paolo Marchetti, Marianna Nuti, Elisabetta Ferretti, Aurelia Rughetti and Lorenzo Farina. **DNA Damage Response and Repair (DDR) Gene Mutations as an alternative mechanism to generate high TMB in never**

smokers NSCLC patients. *ESMO 2022.* Published in *Annals of Oncology*, VOLUME 33, SUPPLEMENT 7, S1047, SEPTEMBER 2022. DOI: https://doi.org/10.1016/j.annonc.2022.07.1207. **Poster**.

Funding and awards

1) "**Merit Award and Travel Grant**" at "ESMO Immuno-Oncology Congress 2020", 12-19 December 2020, Geneva, Switzerland, with the abstract: "IgM-Rheumatoid Factor as a novel biomarker for a reduced survival in anti-PD-1 treated NSCLC patients through the decrease of CD137+ T cells".

2) "Avvio alla Ricerca" grant as P.I. of the project: "A NETWORK ANALYSIS APPROACH TO PROBE THE ROLE OF CD137+ T CELLS IN GLIOBLASTOMA". Sapienza University of Rome, 2022.

Workshops and seminars

1st YEAR (November 2020 – October 2021).

- Conferenze "Immuno Oncology Program, Reasearch in progress". Novembre 2020 – Ottobre 2021.
- Flow Cytometry and Cell Sorting seminar and training held by Flow Core of Moffitt Cancer Center. November 2020.
- ESMO Immuno-Oncology Congress 2020, Geneva, Switzerland, 9-12 December 2020.
- Master Immunoncology III: New therapeutic pathways: 22-23 aprile 2021: Speaker Proff. G. Bernardini, R. Galandrini, Dott. S. Scagnoli ("Sapienza") Prof. M.C. Merlano, Candiolo IRCCS (TO); Prof. I. Ruscito, ("Sapienza") Prof. F. Marampon ("Sapienza") Prof. P. Lucatelli (Pol.Umberto I, Roma).
- Introduzione a R parte I: elementi base di R, gli oggetti di R, variabili, strutture dati e di controllo, funzioni, caricamento dati, esportazione dati, esempi applicativi. Dr. Giulia Fiscon (CNR, FMP).
- Master Immunoncology IV: IMMUNONCOLOGIA E PRINCIPALI NEOPLASIE 13-14 maggio 2021.
- Lectio magistralis Network Medicine: Approach to the definition, Diagnosis, and treatment of Disease in the Era of Precision Medicine 10 Maggio 2021.
- Principi e applicazioni di NGS e citofluorimetria a flusso. Prof.ssa E. Ferretti e prof.ssa C. Napoletano 26 Maggio 2021.
- Prof. R. Pfister "Personalized Pediatric Oncology in 2021". 9 Giugno 2021.
- Landscapes in oncologia, PRECISION MEDICINE: "targeted therapy" e immunoterapia.

- Master Immunoncologia V: IMMUNONCOLOGIA E PRINCIPALI NEOPLASIE 17-18 Giugno 2021.
- Prof. M. Loda "Role of the microenvironment in prostate cancer progression" 30th Giugno 2021.
- Introduzione a R parte II: analisi dati con R, script, grafici, discussione principali librerie R per analisi dati e di reti, esempi applicativi. Dr Giulia Fiscon (CNR, FMP).
- Master Immunoncologia VI: Autoimmunità e Tumori 8-9 Luglio 2021.
- Master Immunoncology VII: From precision medicine to tailored immunity 23-24 settembre 2021.

2nd YEAR (November 2021 – October 2022).

- Tutti i Martedì, Novembre 2021 – Ottobre 2022. Conferenze "Immuno Oncology Program, Reasearch in progress".
- Tutti i Giovedì, Novembre 2021 – Ottobre 2022. Conferenze "Advances in Tumor Immunology and Cancer Research Journal Club".
- Mercoledì 1 dicembre. Prof.L.Farina/A.Rughetti/M.Nuti, Journal Club su https://doi.org/10.1371/journal.pmed.1003736.
- Mercoledì 15 dicembre. Prof.L.Farina/A.Rughetti/Z.M. Besharat, Journal Club su https://doi.org/10.1371/journal.pmed.1003736.
- Mercoledì 12 gennaio. Prof.L.Farina/A.Rughetti/M.Nuti, Data Base PhD game, Corso per il disegno e costruzione di un database per la raccolta dati dei pazienti e la successiva analisi.
- Giovedì 13 gennaio. Prof. Anthony Fauci, Lectio Magistralis "Covid-19: lessons learned and remaining challenges" del prof. Anthony Fauci in occasione del conferimnto del PhD Honoris Causa in in Advances in infectious diseases, microbiology, legal medicine and public health sciences".
- Mercoledì 19 gennaio. Prof.L.Farina/A.Rughetti/M.Nuti, Network medicine: Perspectives 1.
- Giovedi 20 gennaio. Dr Wendy Campana, School of Medicine, UCSD, La Jolla, CA, USA "Functional Role and Therapeutic Targeting of Exosomes in Nerve Injury".
- Mercoledì 26 gennaio. Prof.L.Farina/A.Rughetti/M.Nuti, Data Base PhD game, Corso per il disegno e costruzione di un database per la raccolta dati dei pazienti e la successiva analisi.
- Martedì 1 febbraio. Prof. Teresa Numerico, Seminari STITCH, "Big data e medicina: vecchie incomprensioni e nuove alleanze".
- Mercoledì 2 Febbraio. Prof.L.Farina/A.Rughetti/M.Nuti Network medicine: Perspectives 2.
- Mercoledì 9 Febbraio. Maura Gancitano e Andrea Colamedici, Seminari STITCH "Big data e medicina"." Prove di dialogo tra medicina e big data: vecchie incomprensioni e nuove alleanze".
- Mercoledì 16 febbraio 14,30-17 online Prof.L.Farina/A.Rughetti/E. Ferretti, Data Base PhD game, Corso per il disegno e costruzione di un database per la raccolta dati dei pazienti e la successiva analisi.
- Giovedi 17 febbraio. A.Rughetti, Basic of Immunology for Oncology – I.

- Venerdì 18 febbraio. A.Rughetti Basic of Immunology for Oncology – II.
- Mercoledì 23 febbraio. Prof.L.Farina/A.Rughetti/M.Nuti, Data Base PhD game, Corso per il disegno e costruzione di un database per la raccolta dati dei pazienti e la successiva analisi.
- Mercoledì 2 Marzo. Prof.L.Farina/A.Rughetti/M.Nuti, Network medicine: Perspectives 3.
- Mercoledì 9 Marzo. Prof.L.Farina/A.Rughetti/A.Po, Data Base PhD game, Corso per il disegno e costruzione di un database per la raccolta dati dei pazienti e la successiva analisi.
- Mercoledì 16 marzo. Prof.L.Farina/A.Rughetti/Z.M. Besharat/A. Po/E. Ferretti, Data Base PhD game, Corso per il disegno e costruzione di un database per la raccolta dati dei pazienti e la successiva analisi.
- Mercoledì 23 Marzo. Prof.M.Petti/L.Farina, I linguaggi della Network medicine.
- Mercoledì 30 marzo. Prof.M.Petti/L.Farina, I linguaggi della Network medicine.
- Mercoledì 6 Aprile. Prof.L.Farina/A.Rughetti/A.Po, Data Base PhD game, Corso per il disegno e costruzione di un database per la raccolta dati dei pazienti e la successiva analisi.
- Mercoledì 13 Aprile. Prof.M.Petti/L.Farina, I linguaggi della Network medicine.
- Mercoledì 20 Aprile. Prof.M.Petti/L.Farina, I linguaggi della Network medicine.
- Mercoledì 27 Aprile. Prof.M.Petti/L.Farina, I linguaggi della Network medicine.
- Mercoledì 4 maggio. Prof.L.Farina/A.Rughetti/Z.M. Besharat/A. Po/E. Ferretti, Data Base PhD game, Corso per il disegno e costruzione di un database per la raccolta dati dei pazienti e la successiva analisi.
- Mercoledì 18 maggio. Prof.L.Farina/A.Rughetti/Z.M. Besharat/A. Po/E. Ferretti, Data Base PhD game, Corso per il disegno e costruzione di un database per la raccolta dati dei pazienti e la successiva analisi.
- Mercoledì 25 maggio. Prof.L.Farina/A.Rughetti/Z.M. Besharat/A. Po/E. Ferretti, Tutoring: Learned lessons 36° vs 37°.
- Mercoledì 8 giugno. Prof.L.Farina/A.Rughetti/Z.M. Besharat/A. Po/E. Ferretti, Data Base PhD game, Corso per il disegno e costruzione di un database per la raccolta dati dei pazienti e la successiva analisi.
- Mercoledì 22 Giugno. Prof.L.Farina/A.Rughetti/Z.M. Besharat/A. Po/E. Ferretti, Data Base PhD game, Corso per il disegno e costruzione di un database per la raccolta dati dei pazienti e la successiva analisi.
- Mercoledì 6 luglio. Prof.L.Farina/A.Rughetti/Z.M. Besharat/A. Po/E. Ferretti, Data Base PhD game, Corso per il disegno e costruzione di un database per la raccolta dati dei pazienti e la successiva analisi.
- Mercoledì 20 luglio. Prof.L.Farina/A.Rughetti/Z.M. Besharat/A. Po/E. Ferretti, Data Base PhD game, Corso per il disegno e costruzione di un database per la raccolta dati dei pazienti e la successiva analisi.

3rd YEAR (November 2022 – October 2023).

- Tutti i Martedì, Novembre 2022 – Ottobre 2023. Conferenze "Immuno Oncology Program, Reasearch in progress".

- Tutti i Giovedì, Novembre 2022 – Ottobre 2023. Conferenze "Advances in Tumor Immunology and Cancer Research Journal Club".
- Me 21 Settembre 2022. L.Farina- A.Rughetti- A.Po- M.Petti- C.Napoletano- E.Ferretti Meeting PhD students.
- Me 5 Ottobre 2022. Dottorandi 3° anno European Society for Medical Oncology 2022 update.
- Lu 17 Ottobre 2022. L.Farina- A.Rughetti- A.Po-Z.M.Besharat - E.Ferretti Passaggio d'anno.
- 16 Novembre 2022. Therapeutic Development in Neuro-Oncology Symposium.
- 14 Dicembre 2022. Jennifer L. Guerriero, PhD, Dana-Farber Cancer Institute, presents "The complexities of tumor associated macrophages and the key to effective targeting for anti-cancer therapy." Seminar and lunch with speaker.
- 14 Febbraio. Thirumala-Devi Kanneganti, PhD, St. Jude Children's Research Hospital, presents "Targeting Innate Immunity and Inflammatory Cell Death, PANoptosis for the Treatment of Inflammatory and Infectious Diseases." Seminar and lunch with speaker.
- Ma 14 Marzo 2023. Z.M. Besharat. Come si allestisce un data-base (1/2).
- Ve 17 Marzo 2023. Z.M. Besharat. Come si allestisce un data-base (1/2).
- Tutti i Venerdì, Marzo 2023 – Luglio 2023. Gruppo di lavoro B - l'applicazione della medicina delle reti nell'ambito oncologico. L.Farina- A.Rughetti- A.Po- M.Petti- C.Napoletano- E.Ferretti.
- Ma 9 maggio 2023. A. Po - G. Catanzaro. Modelli preclinici 1/2.
- Ma 16 maggio 2023 . A. Po - G. Catanzaro. Modelli preclinici 2/2.
- 13 Giugno. Weiping Zou, MD, PhD, University of Michigan Medical School, presents "IFN, a matter of life and death in cancer immunotherapy."
- 26 Luglio. Juan R. Cubillos-Ruiz, PhD, Meyer Cancer Center, Weill Cornell Medicine, Cornell University, presents "Decoding and Intercepting ER Stress Signals for Cancer Immunotherapy." Seminar and lunch with speaker.